Dual-specificity phosphatases 13 and 27 as key switches in muscle stem cell transition from proliferation to differentiation

Takuto Hayashi[1], Shunya Sadaki[1,2], Ryosuke Tsuji[1,2], Risa Okada[3], Sayaka Fuseya[1,4], Maho Kanai[1], Ayano Nakamura[1,5], Yui Okamura[1,5], Masafumi Muratani[6], Gu Wenchao[7], Takehito Sugasawa[8], Seiya Mizuno[9], Eiji Warabi[1], Takashi Kudo[1], Satoru Takahashi[1*], Ryo Fujita[10, *]

[1] Laboratory Animal Resource Center in Transborder Medical Research Center, and Department of Anatomy and Embryology, Institute of Medicine, University of Tsukuba, Ibaraki 305-8575, Japan

[2] Ph.D. Program in Humanics, School of Integrative and Global Majors, University of Tsukuba, Ibaraki 305-8575, Japan

[3] JEM Utilization Center, Human Spaceflight Technology Directorate, Japan Aerospace Exploration Agency (JAXA), Ibaraki 305-8505, Japan

[4] Cellular and Molecular Biotechnology Research Institute, National Institute of Advanced Industrial Science and Technology, Ibaraki 305-8565, Japan

[5] College of Medicine, School of Medicine and Health Sciences, University of Tsukuba, Ibaraki 305-8575, Japan

[6] Department of Genome Biology, Transborder Medical Research Center, Institute of Medicine, University of Tsukuba, Ibaraki 305-8575, Japan

[7] Department of Diagnostic and Interventional Radiology, Institute of Medicine, University of Tsukuba, Ibaraki 305-8575, Japan

[8] Laboratory of Clinical Examination and Sports Medicine, Department of Clinical Medicine, Institute of Medicine, University of Tsukuba, Ibaraki 305-8575, Japan

[9] Laboratory Animal Resource Center in Transborder Medical Research Center, and Department of Laboratory Animal Science, Institute of Medicine, University of Tsukuba, Ibaraki 305-8575, Japan.

[10] Division of Regenerative Medicine, Transborder Medical Research Center, Institute of Medicine, University of Tsukuba, Ibaraki 305-8575, Japan

Running head: Loss of Dusp 13 and 27 Delays Muscle Regeneration

***Correspondence:**

Ryo Fujita, Ph.D.

Division of Regenerative Medicine, Transborder Medical Research Center, Institute of Medicine, University of Tsukuba, Ibaraki 305-8575, Japan.

E-mail: fujiryo@md.tsukuba.ac.jp

TEL: +81-29-853-7516

Satoru Takahashi, M.D., Ph.D.
Laboratory Animal Resource Center in Transborder Medical Research Center, and Department of Anatomy and Embryology, Institute of Medicine, University of Tsukuba, Ibaraki 305-8575, Japan
E-mail: satoruta@md.tsukuba.ac.jp

Significance Statement

MYOD protein is not expressed in quiescent muscle stem cells but accumulates rapidly following muscle injury, leading to the proliferation of myogenic progenitors for differentiation. However, the direct targets of MYOD, aside from myogenin, which play roles in myogenic differentiation remain incompletely understood. Using previously established MyoD knock-in mice and single-cell RNA sequencing, we discovered that Dusp13 and Dusp27 are potential target genes of MYOD that promote myogenesis during muscle regeneration in adult mice.

Abstract

Muscle regeneration depends on muscle stem cell (MuSC) activity. Myogenic regulatory factors, including myoblast determination protein 1 (MyoD), regulate the fate transition of MuSCs. However, the direct target of MYOD in the process is not completely clear. Using previously established MyoD knock-in (MyoD-KI) mice, we revealed that MyoD targets dual-specificity phosphatase (Dusp) 13 and Dusp27. In *Dusp13*:*Dusp27* double knock-out (DKO) mice, the ability for muscle regeneration after injury was reduced. Moreover, single-cell RNA sequencing of MyoD-high expressing MuSCs from MyoD-KI mice revealed that *Dusp13* and *Dusp27* are expressed only in specific populations within MyoD-high MuSCs, which also express *Myogenin*. Overexpressing *Dusp13* in MuSCs causes premature muscle differentiation. Thus, we propose a model where DUSP13 and DUSP27 contribute to the fate transition of MuSCs from proliferation to differentiation during myogenesis.

Keywords: Muscle stem cell, MyoD, Dual specificity phosphatase 13:27, Regeneration, Single-cell RNA-sequencing

Introduction

Skeletal muscle stem cells (MuSCs) [1] play a vital role in postnatal muscle development and skeletal muscle regeneration [2]. MuSCs are located near the myofibers beneath the basal lamina and exist in a quiescent state in healthy muscle under resting conditions. However, in response to injury, they become activated, differentiate, and generate new myofibers [3,4]. Some of the progeny of the activated MuSCs undergo self-renewal to perpetually sustain the MuSC pool throughout a lifespan [5–7].

The dynamics of MuSCs are regulated intricately by a series of myogenic regulatory factors (MRFs) that are expressed sequentially during myogenesis. Quiescent MuSCs express the paired homeodomain family transcription factor PAX7 [8,9]. Loss of Pax7 results in normal embryonic and fetal myogenesis but reduced postnatal muscle growth [9]. Interestingly, MuSCs are present in Pax7 mutants, although the population decreases progressively as mice mature due to cell cycle defects and apoptosis [10,11]. The MRFs, including MyoD, Myf5, myogenin, and MRF4, act as basic helix–loop–helix (bHLH) transcription factors that bind to E-box sites. MYOD and MYF5 are essential transcription factors for muscle lineage specification [12,13], MYOGENIN and MRF4 are indispensable for muscle differentiation [14,15]. Additionally, MRFs are induced in activated MuSCs during muscle regeneration in adult mice. Quiescent MuSCs repress the translation of specific transcripts that keep them primed to rapidly activate the myogenic program in case of injury [16]. MicroRNAs and RNA-binding proteins primarily mediate the repression of *Myf5* and *MyoD* transcripts [17–20]. Upon injury, the block on translation is lifted, leading to the rapid translation of *MyoD* and *Myf5*, initiating the myogenic program for regeneration.

MyoD KO mice exhibited delayed myogenic differentiation and accelerated self-renewal ability in MuSCs. Furthermore, *MyoD* KO mice on an mdx background, a model for Duchenne muscular dystrophy, have a low survival rate [21,22] . MYOD plays a critical role in determining the fate of activated MuSCs by balancing self-renewal and differentiation during myogenesis. However, the direct targets of MYOD, apart from *myogenin* that play critical roles in myogenic differentiation, are not completely understood.

In a prior study, we established a MyoD knock-in (KI) reporter mouse line to recapitulate the expression levels of endogenous MyoD using tdTomato fluorescence [23]. The fluorescence allowed us to identify the status of MuSCs during myogenesis. We observed that the MyoD-low population, characterized by low tdTomato fluorescence, consisted mostly of undifferentiated stem-like cells. Conversely, the MyoD-high population, with high tdTomato fluorescence, exhibited features of committed and differentiating MuSC [23]. To investigate the molecular mechanisms governing the stemness and commitment/differentiation of MuSCs, whole-transcriptome data were collected from MyoD-low MuSCs, MyoD-high MuSCs, and quiescent MuSCs isolated from $Pax7^{YFP/YFP}$ (Pax7-YFP) mice [23,24]. The establishment of MyoD-KI mice and the availability of whole-transcriptome data

105 at different activation stages of MuSCs based on MYOD levels provide a valuable platform for
106 understanding the fate determination mediated by MYOD.
107 The DUSP family comprises members of the protein tyrosine phosphatase superfamily involved in
108 the dephosphorylation of phosphotyrosine and phosphoserine/threonine residues [25–27]. They
109 interact directly with MAPK effectors, including extracellular signal-regulated kinases 1/2 (ERK1/2),
110 leading to their dephosphorylation and subsequent inactivation. Therefore, DUSPs play regulatory
111 roles in cell growth, cell differentiation, and apoptosis [28–30]. The phosphatase domain common to
112 DUSPs is known as protein tyrosine phosphatases (PTP). DUSPs can be classified into two
113 subfamilies based on the presence or absence of the MAP kinase-binding (MKB) motif or the kinase-
114 interacting motif (KIM). The DUSPs with the KIM domain are classified as typical DUSPs, whereas
115 those lacking the KIM domain are classified as atypical DUSPs [31,32].
116 The functional regulation of substrates by DUSPs does not always require phosphatase activity.
117 DUSPs can control the function of MAPKs by sequestering them in the cytoplasm or nucleus. It has
118 also been observed that some DUSPs are catalytically inactive [33]. For example, DUSP27 lacks
119 phosphatase activity due to the absence of a highly conserved cysteine residue essential for enzyme
120 activity [34]. Nevertheless, the loss of *Dusp27* in zebrafish leads to severe disorganization of the
121 sarcomere structure, underscoring the significance of its pseudophosphatase function in muscle
122 development [34]. Within skeletal muscles, DUSP5 and DUSP6, classified as typical DUSPs, regulate
123 muscle hypertrophy and myofiber types by inhibiting ERK1/2 signaling [35]. However, our
124 understanding of the function of atypical DUSPs in skeletal muscle in mammals is limited.
125 In the present study, we used our MyoD-KI transcriptome and various datasets to identify *Dusp13*
126 as a direct target for MYOD. *Dusp13* is located on chromosome 10a22.2 and encodes two distinct
127 DUSPs, *Dusp13a* and *Dusp13b*. Although DUSP13a is expressed predominantly in murine skeletal
128 muscles [36], its specific roles in skeletal muscle remain unclear. Single KO of *Dusp13* did not exhibit
129 any regenerative defects; however, there was compensatory upregulation of *Dusp27* in skeletal
130 muscles lacking *Dusp13*. To further investigate, we generated a double KO (DKO) of *Dusp13* and
131 *Dusp27* and observed diminished muscle regeneration activity after acute muscle injury. Furthermore,
132 through single-cell RNA-seq (scRNA-seq) analysis, we found that the expressions of *Dusp13* and
133 *Dusp27* are limited to specific subsets of MyoD-high expressing MuSCs that also show the expression
134 of late myogenic markers. Based on the findings, we propose a model in which DUSP13 and DUSP27
135 instigate the transition of MuSCs from an activated/proliferative state to a differentiation state during
136 regeneration.
137

138 ## Materials and Methods

139 **Mice**

Mice were kept in a specific pathogen-free environment at the Laboratory Animal Resource Center at the University of Tsukuba, Ibaraki, Japan. All experiments were performed in compliance with the relevant Japanese and institutional laws and guidelines and were approved by the University of Tsukuba Animal Ethics Committee (authorization number: 23-046). The study used 10–15-week-old C57BL/6 J male and female WT, *Dusp13* KO, *Dusp27* KO, and *Dusp13*/*Dusp27* DKO mice, unless otherwise stated. Quiescent MuSCs were isolated directly from the leg muscles of 15–16-week-old male Pax7-YFP (*Pax7*$^{YFP/YFP}$) [24] [23]. The TA muscle was acutely injured by injecting 50 μL of 10 μM cardiotoxin (Funakoshi Co., Ltd., Tokyo, Japan) under anesthesia using isoflurane inhalation.

Generation of *Dusp13* and *Dusp27* KO mice

The *Dusp13* and *Dusp27* KO mice were generated using the CRISPR/Cas9 system. Two target sgRNAs were designed as follows; 5′-GTAGGGTTCACACAGAACGG-3′ and 5′-ATGTCACAGTAAGCGTACGG-3′ for targeting all exons of the *Dusp13* gene on mouse chromosome 14, and 5′-GCATCCTTCCACATCAACCC-3′ and 5′-GGTAAGGGTGCTCTCGACAA-3′ for targeting regions located in introns 2 and 3, respectively, of the *Dusp27* gene on mouse chromosome 1. Each target sgRNA was cloned into the guide RNA-Cas co-expression plasmid px330-U6-Chimeric_BB-CBh-hSpCas9 vector (Addgene, Watertown, MA, USA). A mixture of the four cloned plasmids was microinjected into the pronuclei of C57BL/6 J fertilized eggs, and living embryos were transferred to pseudo-pregnant ICR female mice. Genomic DNA screening was performed using PCR with the primers and protocols listed in Table S1.

Muscle stem cell isolation and culture

MuSCs were isolated from the hindlimb muscles of 11–13-week-old mice following MACS using a Satellite Cell Isolation Kit (Miltenyi Biotec, Bergisch Gladbach, Germany) and anti-integrin α7 microbeads (Miltenyi Biotec), as previously described [23]. The adult hindlimb muscles were minced in ice-cold Ham's F12 medium. The minced muscles were then incubated in 0.1% collagenase D (Roche, Basel, Switzerland) and 0.1% trypsin in Ham's F12 (Gibco, Waltham, MA, USA) with 1% penicillin-streptomycin for 45 min at 37 °C on a shaker for three rounds of digestion. After each round, the supernatant was collected in a 50 mL tube containing 8 mL of fetal bovine serum (FBS) (Gibco) on ice, and fresh 0.1% trypsin/0.1% collagenase digestion buffer was added to the tube for the next round of digestion. The collected supernatant was filtered through a sequence of 100 and 40 μm nylon mesh strainers and then centrifuged at 400 × *g* for 10 min at 4 °C. The pellets were resuspended in PBS containing 2% FBS and processed for MACS or flow cytometry. The MuSCs were cultured in a growth medium containing 39% DMEM (Gibco), 39% Ham's F12, 20% FBS (Gibco), and 1% UltroserG (Pall Life Sciences, Port Washington, NY, USA). Differentiation media consisted of 2%

horse serum in Dulbecco's modified Eagle's medium (DMEM). Gelatin (0.2%)-coated dishes were used for MuSC culture unless otherwise indicated.

Flow cytometry analysis and cell sorting

MACS-isolated MuSCs were cultured for 5 days. They were detached using 0.25% trypsin/EDTA, then centrifuged and resuspended in 2% FBS/PBS. Propidium iodide (PI) was added to the cells at a 1:500 (vol/vol) ratio and incubated on ice for 10 min. The cells were either analyzed using a flow cytometer (CytoFLEX S; Beckman Coulter, Brea, CA, USA) or sorted using a MoFlo XDP flow cytometer (Beckman Coulter). Debris and dead cells were excluded using forward scatter, side scatter, and PI gating. Gates were defined based on WT control fluorescence. The data were analyzed using FlowJo™ software ver. 10.7.1 (BD Biosciences, Franklin Lakes, NJ, USA).

Immunofluorescence and histological analysis

Cultured cells were washed twice with PBS after removing the media and fixed with 4% paraformaldehyde (PFA) for 15 min. The fixed cells were blocked with 2% BSA/PBS for 1 h at room temperature and then washed three times with PBS. Isolated single EDL myofibers [6] were fixed using 2% PFA for 15 min, permeabilized with 0.1% Triton in PBS, and blocked with 5% goat serum in 0.1% Triton/PBS for 30 min on a shaker. The cultured cells and single EDL myofibers were incubated with primary antibodies at 4 °C overnight. The myotube diameter and nucleus number were measured using the ImageJ software (NIH, Bethesda, MI, USA). The myotube diameter was defined as the average diameter at the three ends (both ends and the center) for each MYHC-positive and multinucleated myotube. TA muscles were neatly stacked on top of each other. The Achilles tendon side was vertically mounted on tragacanth gum on a cork disc and quickly frozen in isopentane cooled in liquid nitrogen. Thin frozen muscle sections (8 μm) were subjected to immunohistochemical analyses. The sections were fixed with 4% PFA for 10 min at room temperature. For PAX7 staining, sections underwent antigen retrieval with DAKO buffer (Agilent, Santa Clara, CA, USA) for 10 min at 110 °C, followed by blocking with M.O.M. blocking reagent (Vector Laboratories, Newark, CA, USA). The sections were then incubated with primary antibodies overnight at 4 °C. Tissue sections were mounted with VECTASHIELD Vibrance Antifade Mounting Medium with DAPI (Vector Laboratories). Primary antibodies were against PAX7 (Developmental Studies Hybridoma Bank (DSHB)), MYOD (sc-377460; SantaCruz), MYOD (ab133627, abcam), RFP (600-401-379, Rockland), LAMININ (sc-59854; SantaCruz), MYOGENIN (124800; Abcam, Cambridge, UK), MYOGENIN (MA5-11486; Invitrogen, Waltham, MA, USA), (MyHC (DSHB; MF20), and KI67 (MA5-14520; Invitrogen, Waltham, MA, USA). For immunofluorescence, secondary antibodies conjugated with Alexa Fluor-488, Alexa Fluor-546, Alexa Fluor-555, Alexa Fluor-633, and Alexa Fluor-647 were used. The secondary antibodies included anti-mouse IgG1, anti-mouse IgG2b, anti-

211 rat IgG, and anti-rabbit antibodies (Thermo Fisher Scientific, Waltham, MA, USA). For HE staining,
212 the SOL, PLA, and TA muscle sections were stained with Mayer's hematoxylin (Wako, Richmond,
213 VA, USA) for 10 min. After washing in warm running tap water (50 ± 5 °C) for 3 min, eosin (Wako)
214 was applied for 1 min. The sections were then dehydrated using two changes (5 s each) of 95% ethanol
215 and two changes (5 s each) of 100% ethanol (Wako), followed by three changes of xylene (Wako) for
216 5 min each. Finally, the sections were mounted with DPX mounting medium (Sigma-Aldrich, St.
217 Louis, MA, USA) and observed with a BIOREVO BZ-X800 microscope (Keyence, Osaka, Japan).
218 The CSA of myofibers was assessed using the same microscope system and a hybrid cell count
219 application (Keyence).
220
221 **RNA-scope**
222 Male Pax7-YFP mice, aged 12–15 weeks, were used to directly isolate quiescent MuSCs from the leg
223 muscles. A total of 20,000 sorted cells were seeded in a well of a 24-well culture plate, pre-coated
224 with iMatrix-511 (Nippi) for 1 h, and immediately fixed with 4% paraformaldehyde (PFA) for 15 min
225 (freshly isolated MuSCs). The sorted cells were cultured in growth medium for 6 days (GM6) or in
226 differentiation medium for 6 days (DM6) and then fixed with 4% PFA for 15 min. For the isolation of
227 MyoD-low and MyoD-high MuSCs, MACS-isolated MuSCs from MyoD-KI mice were cultured for
228 5 days, detached using 0.25% trypsin/EDTA, followed by centrifugation and resuspension in 2%
229 FBS/PBS, as previously described [23]. The cells were sorted using a MoFlo XDP flow cytometer
230 (Beckman Coulter), and dead cells were excluded by propidium iodide (PI) gating. The sorted MyoD-
231 low and MyoD-high MuSCs were seeded in a well of a 24-well culture plate pre-coated with iMatrix-
232 511 (Nippi) for 30 min, then immediately fixed with 4% PFA for 15 min.
233 For the detection of Dusp13 and Dusp27 transcripts, the fixed cells were processed using the
234 RNAscope™ Multiplex Fluorescent V2 Assay (ADC, 323270). Dusp13 and Dusp27 transcripts were
235 hybridized with Mn-Dusp13a-O1-C1 (ADC, 1332391-C1) and Mn-Styxl2 (Dusp27)-C1 (ADC,
236 1332401-C1) probes, respectively. Briefly, the fixed cells were washed twice with PBS. After a 10-
237 minute incubation in hydrogen peroxide solution, the cells were incubated with protease III diluted
238 1:15 in PBS for 10 min. Following two PBS washes, the cells were hybridized with each C1 probe for
239 2 h at 40°C. After the amplification steps in the kit, Dusp13 and Dusp27 transcripts were visualized
240 using the TSA Vivid Fluorophore Kit 520 (R&D Systems, 7523). Finally, the cells were washed twice
241 with PBS, and subsequent immunofluorescence analysis was performed using antibodies against
242 PAX7, MYOD, MF20, and RFP, as described above. Nuclei were counterstained with DAPI.
243
244 **DNA construct**
245 The *MyoD*, *Dusp13*, and *Dusp27* genes were amplified using PrimeStar GXL DNA Polymerase
246 (Takara Bio, Shiga, Japan) with soleus cDNA as the template. After confirming the size of the PCR

247 products using 1% agarose gel electrophoresis, the target PCR product was purified from the gel. The
248 purified DNA fragment of *Dusp13* was digested with EcoRI. The digested fragments were then ligated
249 to pENTR3c-IRES-EGFP, which was also digested with the same restriction enzymes, using Ligation
250 High (TOYOBO, Osaka, Japan). DUSP13 deficient in phosphatase activity (Dusp13_Mut) was
251 generated using the PrimeSTAR® Mutagenesis Basal Kit (Takara Bio). The Dusp family contains the
252 amino acid cysteine, which is essential for enzyme activity [37]. The present mutant was generated
253 using Dusp13_D97A and Dusp13_C128S primers (Table S1) to replace aspartic acid at position 97
254 and cysteine at position 128 with alanine and serine, respectively. The reaction was then transformed
255 into One shot TOP10 Competent cells (Thermo Fisher Scientific) and seeded on kanamycin-LB agar
256 plates. A single colony was grown in kanamycin-LB medium, and after confirming each insert by
257 colony PCR and DNA sequencing, plasmid purification was performed using the FastGene Plasmid
258 Mini Kit. Clones without any mutations in the product were selected. The LR reaction of the Gateway
259 system was performed to recombine pENTR3c-Dusp13-IRES-EGFP into pAd/CMV/V5-DEST
260 (Thermo Fisher Scientific). In total, 100 ng of the purified plasmid and 300 ng of pAd/CMV/V5-DEST
261 were mixed at room temperature and reacted according to the manual for Gateway LR Clonase II
262 Enzyme Mix (Thermo Fisher Scientific). The 5 μL reaction was subsequently transformed into 50 μL
263 of competent cells and seeded on ampicillin-LB agar plates. Single colonies were cultivated in LB
264 medium, and confirmation of the insert was achieved through colony PCR. The confirmed plasmid
265 was prepared in large quantities using the PureLink HiPure Plasmid Midiprep Kit (Thermo Fisher
266 Scientific). The plasmid concentration was measured using a NanoDrop 2000 Spectrophotometer
267 (Thermo Fisher Scientific), and 20 μg of the plasmid was digested with the restriction enzyme PacI.
268 Verification of complete digestion by PacI was performed through 1% agarose gel electrophoresis,
269 and the linearized plasmid was purified via phenol:chloroform extraction and ethanol precipitation.
270 To generate the luciferase vector, the purified DNA fragment of the *MyoD* gene was cloned into a
271 pAAV-CMV vector using the In-Fusion Cloning HD Kit (Takara Bio). The mouse *Pax7 and*
272 *Myogenin* sequence was amplified by PrimeSTAR® Max DNA polymerase (TAKARA) using the
273 primers listed in the Table S1. The purified *Pax7* fragment was cloned into *Bam*HI-*Sal*I site of pLenti-
274 PGK-GFP [38] using In-Fusion cloning HD kit (TAKARA). The purified *Myogenin* fragment was
275 cloned into *Xho I* site of pcDNA-EGFP (gift from Doung Golenbock, Addgene plasmid #13031) using
276 In-Fusion cloning HD kit (TAKARA). The DNA fragment corresponding to the 300 bp 5′ upstream
277 region (−250 to +50) of *Dusp13* or the 1,200 bp upstream region (−1,000 to +200) of *Dusp27* from
278 EDL muscle DNA of C57BL/6 mice was inserted into a pGL4.10 promoter-less luciferase vector
279 (Promega, Madison, WI, USA) digested with XhoI. The resulting constructs were named pGL4-
280 Dusp13 or pGL4-Dusp27. The primer sequences for the construction of vectors are provided in Table
281 S1.
282

Adenovirus production and infection

293A cells were seeded on BD BioCoat Collagen I 60 mm Culture Dishes (IWAKI) using the medium (DMEM and 10% FBS). Purified 5 μg of pAd/CMV/V5-DEST plasmid was transfected using Fugene HD (Promega) when the 293A cells were 80% confluent. When the cells began to float, the bottom surface of the dish was scraped off using a scraper and collected in a 15 mL High-Clarity Polypropylene Conical Tube 17 × 120 mm style (FALCON) (primary virus). The primary virus underwent repeated freeze-thaw cycles in a water bath at 37 °C and in liquid nitrogen. This freeze-thaw process was repeated three times. Finally, it was frozen again and stored at −80 °C. Next, 2 mL of the primary virus was thawed at 37 °C and centrifuged for 15 min at 3,000 rpm (KUBOTA 2800). The supernatant was added to 293A cells (80% confluent) cultured in a 100 mm Collagen-Coated Dish Collagen I (IWAKI) and infected for 1 h at 37 °C in a CO_2 incubator. Then, 8 mL of medium was added. When the cells floated, they were scraped off using a scraper and collected in 15-mL tubes. The freeze-thaw process was repeated three times. Finally, it was frozen again and stored at −80 °C. This virus was created as the 2nd virus. This procedure was repeated five times, and the 5th virus was stored at −80 °C. Next, to purify the virus, the fifth virus was freeze-thawed three times and ultracentrifuged at 23 k rpm at 4 °C for 1.5 h in the Super-centrifuge Optima XE-90 Ultracentrifuge (Beckman Coulter) using Ultra-Clear Centrifuge Tubes (Beckman Coulter). After ultracentrifugation, recombinant adenovirus was extracted from the second viral layer from the bottom. The dialysis buffer was prepared in three heat-resistant plastic bottles by adding 1976 mL of MilliQ, 20 mL of 1 M Tris HCl (pH 8.0), and 4 mL of 1 M $MgCl_2$, and the bottles were then autoclaved. For dialysis, the recombinant adenovirus extract was injected into Slide-A-Lyzer Dialysis Cassettes (Thermo Fisher Scientific) and dialyzed in a dialysis buffer at 4 °C with stirring. The dialysis buffer was changed three times every 12 h. The purified recombinant adenovirus was stored at −80 °C. Infectious titers were measured using the Adeno-X Rapid Titer Kit (Takara Bio). After 48 h from the start of differentiation, the medium was replaced with a fresh DM and incubated with adenovirus at a multiplicity of infection (MOI) of 250 in a differentiation medium. Two days after the virus transduction, the cells were fixed with 4% PFA/PBS.

Luciferase assay

To determine if MyoD, Pax7 and Myogenin could activate the *Dusp13* or *Dusp27* promoter, we co-transfected 100 ng of pGL4-Dusp13 or pGL4-Dusp27 with 50 ng of pRL-TK vectors (Promega) and varying amounts (0, 10, 20, 100, 200 ng) of MyoD, Pax7, and Myogenin expression vectors into 293T cells (Takara Bio) using the FuGENE HD transfection reagent (Promega). Twenty-four hours after transfection, the cells were harvested and assayed using the Dual-Luciferase Reporter Assay System (Promega). Luciferase activity was measured using the GloMax® 20/20 Luminometer (Promega) and normalized based on Renilla luciferase activity from the pRL-TK vector.

Motif enrichment analysis

The presence of Ebox sites in the promoter regions of genes was predicted using the Find Individual Motif Occurrences (FIMO) algorithm from the MEME Suite [39], utilizing the position weight matrix available from JASPAR (https://jaspar.genereg.net/). This analysis was conducted from 1 kbp upstream to 500 bp downstream of the transcriptional start site of *Dusp13*/*Dusp27*.

RNA isolation and RT-qPCR

Total RNA was extracted from various tissues and MuSCs using ISOGEN (NIPPON GENE, Chiyoda, Tokyo, Japan). We synthesized first-strand cDNA using the QuantiTect Reverse Transcription Kit (Qiagen, Hilden, Germany). Polymerase chain reaction (PCR) was then performed using a THUNDERBIRD SYBR qPCR system (TOYOBO) and a TP850 Thermal Cycler Dice Real Time System (Takara Bio, Shiga, Japan). The primer sequences are listed in Table S1. The relative amount of each transcript was normalized to the number of beta-actin transcripts.

Single-cell RNA-seq analysis

MACS-isolated MuSCs from MyoD-KI mice [23] were cultured for five days and then detached using 0.25% trypsin/EDTA. The cells were centrifuged and resuspended in 2% FBS/PBS. The cells were incubated with PI at a 1:500 (v/v) ratio. Debris and dead cells were excluded using forward scatter, side scatter, and PI gating. Live MyoD-tdTomato-high MuSCs were sorted using a MoFlo XDP flow cytometer (Beckman Coulter) based on our previous study's gate of MyoD-tdTomato-high population. Single RNA-seq libraries from MyoD-tdTomato-high MuSCs were generated using a chromium controller (10× Genomics, Pleasanton, CA, USA) following the manufacturer's instructions. Approximately 10,000 cells were processed using the Chromium Next GEN Single Cell 3'Reagent Kits v3.1 (10× Genomics). The sequencing was performed on a NovaSeq 6000 (Illumina, San Diego, CA, USA) operated by the Rhelixa Corporation (Tokyo, Japan). The fastq files were processed using default parameters for adaptor sequence filtering, and low-quality reads were removed to obtain clean data. Feature-barcode matrices were then generated by aligning the reads to the mouse genome (mm10 Ensemble: version 92) with CellRanger v3.1.0. The scRNA-seq data was processed using the standard Seurat pipeline. For quality control, the range of gene reads per cell was set between 300 and 6000. Additionally, the filtering threshold for mitochondrial gene proportion was established at 15%. The "FindVariableFeature" function was used to determine the highly variable genes. Cell clustering was determined using the "FindNeighbors" and "FindCluster" functions in the Seurat package. To investigate the proliferation of genes involved in the development of muscle stem cells, the "Monocle2" package was applied for conducting pseudotime analysis. The biological function

354 analysis was performed using GO analysis. The scRNA-seq data have been deposited under accession
355 number GSE250228.
356
357 **Quantification and statistical analysis**
358 All data are represented as the mean of biological replicates, with individual sample data shown as
359 dots. Values are reported as mean ± standard error of the mean (SEM). Statistical analyses were
360 performed using unpaired Student's t-tests or non-repeated measures analysis of variance (ANOVA),
361 followed by Tukey's test, using GraphPad Prism (GraphPad Software, Inc., San Diego, CA, USA). P
362 values for statistical significance are indicated as * $P < 0.05$, ** $P < 0.01$, *** $P < 0.001$, not detected
363 (n.d.), or not significant (n.s.).
364
365

366 **Results**

367 ***Dusp13 is directly regulated by MyoD activity.***

368 We previously generated MyoD-KI mice that allow us to assess MYOD expression through tdTomato
369 fluorescence intensity [23]. To identify new regulators directly controlled by MYOD activity, we
370 utilized RNA-seq data from MyoD-low and MyoD-high expressing MuSCs from the MyoD-KI mice,
371 as well as freshly isolated quiescent MuSCs from Pax7$^{YFP/YFP}$ (Pax7-YFP) mice (Figure 1A). Initially,
372 we visualized the differentially expressed genes (FDR < 0.05) between the MyoD-low and MyoD-
373 high populations using a heatmap (Figure 1A). We found that 966 genes were significantly
374 upregulated as *MyoD* levels increased (MyoD-KI Cluster2). To further narrow down the targets, we
375 consulted a gene expression database of proliferating and differentiating MuSCs from *MyoD* KO mice
376 [40]. We identified 1797 genes that were not upregulated in *MyoD* KO mice (MKO Cluster2 in Figure
377 1B). Through a Venn diagram comparison, we combined 505 genes from the MyoD-KI and MKO
378 clusters. Additionally, when we included *MyoD* ChIP-seq data from ChIP-Atlas, we found that 35
379 genes were enriched (Figure 1C) [41,42]. Finally, out of these 35 genes, six genes (*Ank1*, *Dmpk*,
380 *Dusp13*, *Jsrp1*, *Rapsn*, and *Stac3*) were induced by *MyoD* overexpression in mouse embryonic
381 fibroblasts (MEFs) [43] (Figure 1C and 1D; Figure S1A and S1B). We also confirmed that *Dusp13*
382 mRNA was predominantly enriched in the quadriceps muscles compared to other tissues (Figure S2A).
383 Due to the modulation of *Dusp13* expression by *MyoD levels* (Figure 1E–1H), we analyzed Dusp13
384 mRNA expression in sorted MyoD-low and -high MuSCs from MyoD-KI mice by RNAscope
385 fluorescent in situ hybridization. Dusp13 RNA puncta were not obviously visible in MyoD-low, but
386 accumulated in MyoD-high MuSCs (Figure S3A).

387 In addition, we identified a highly conserved E-box site 150 bp upstream of the transcription
388 initiation site of *Dusp13*, according to the UCSC Genome Browser (Figure 1I). To determine if
389 MYOD binds to the E-box of *Dusp13*, we ligated the putative E-box site of *Dusp13* to a pGL4.10
390 vector to generate a luciferase-*Dusp13*-E-box vector. We then co-transfected the plasmid with a *MyoD*
391 expression vector into the HEK293T cell line. The luciferase activity was significantly upregulated in
392 the presence of *MyoD* when the *Dusp13*-Ebox was present (Figure 1J). In contrast, the luciferase
393 activity was not upregulated in the presence of *Pax7* or *Myogenin* (Figure S2C and S2D). These results
394 suggest that *Dusp13* is a new target of MYOD during myogenesis.

395

396 ***Single Dusp13 or Dusp27 KO mice exhibits no abnormality in muscle development or regeneration.***

397 To investigate the role of DUSP13 in skeletal muscle, we generated *Dusp13* KO mice using CRISPR-
398 Cas9 technology. We confirmed that *Dusp13* expression in skeletal muscle was depleted in these
399 *Dusp13* KO mice (Figure S2E). The *Dusp13* KO mice were born according to Mendelian laws and
400 grew normally, similar to the litter mate wild type (WT) control mice, with respect to body weight and
401 muscle cross-sectional area (CSA) of the soleus (SOL) and plantaris (PLA) muscles (Figure 2A–2C).

402 The number of PAX7+ MuSCs in *Dusp13* KO mice is identical with WT mice (Figure 2D and 2E).
403 We then investigated the regenerative ability in the *Dusp13* KO mice. We injected cardiotoxin (CTX)
404 into the tibialis anterior (TA) muscles of both WT and *Dusp13* KO mice and no significant histological
405 differences were observed in the CSA of the damaged myofibers with central nuclei at day 7 after the
406 injury (Figure 2F and 2G). Furthermore, immunohistochemical analysis for PAX7 and MYOGENIN
407 showed that the number of PAX7 or MYOGENIN (+) nuclei was similar between WT and *Dusp13*
408 KO mice (Figure 2H–2K). The findings indicate that there is no significant impairment of muscle
409 regeneration in the absence of *Dusp13*.
410 We hypothesized that other members of the *Dusp* family expressed in skeletal muscles could
411 compensate for the function of DUSP13 upon *Dusp13* deletion. Within overlapping genes between
412 the MyoD-KI Cluster 2 and MKO Cluster 2 in Figure 1A and 1B, we identified *Dusp27* as another
413 member of the *Dusp* family that is expressed abundantly in the quadriceps muscles and the heart
414 (Figure S2B). *Dusp27* expression was significantly higher in *Dusp13* KO muscles compared to WT
415 muscles, suggesting compensatory induction following the loss of *Dusp13* (Figure 3A). We also
416 observed a significant increase in *Dusp27* expression when *MyoD* expression increased (Figure 3B,
417 Figure S3B), similar to *Dusp13* (Figure 1F, Figure S3A). Interestingly, we found a potential E-box
418 site located 10 bp upstream of the transcription initiation site of *Dusp27*, which is highly conserved
419 among multiple mammalian species (Figure 3C). The luciferase activity of luciferase-Dusp27-E-box
420 was upregulated significantly in the presence of *MyoD* (Figure 3D) but not in the presence of *Pax7* or
421 *Myogenin* (Figure S2C and S2D), suggesting that both *Dusp13* and *Dusp27* are regulated directly by
422 MYOD activity. To test our hypothesis that DUSP27 compensates for the loss of *Dusp13*, we first
423 generated *Dusp27* KO mice using CRISPR-Cas9. We confirmed the deletion of the gene through
424 qPCR analysis (Figure S2F). Similar to the *Dusp13* KO mice, the *Dusp27* KO mice did not show any
425 differences in body weight (data not shown), myofiber CSA in intact muscles (Figure 3E-H), number
426 of PAX7+ MuSCs in intact muscles (Figure 3I and 3J), myofiber CSA after muscle CTX injury (Figure
427 3K and 3L), and the number of myogenic populations labeled by either PAX7 or MYOGENIN after
428 CTX injury (Figure 3M–3P). These results demonstrate that neither *Dusp13* nor *Dusp27* deficiency
429 influences muscle development and acute muscle regeneration.
430
431 ***Muscle regeneration is delayed in Dusp13:Dusp27 DKO mice.***
432 To investigate the role of DUSP13 and DUSP27 in skeletal muscles, we generated DKO mice. The
433 body weights and muscle weights of DKO mice were found to be similar to those of age-matched WT
434 mice (Figure S4A and S4B). Furthermore, both the SOL and PLA muscles exhibited normal myofiber
435 size (Figure S4C–S4E), and the number of MuSCs (Figure S4F-I) in DKO mice was also normal, as
436 in WT mice. However, histological analysis on days 3, 7, and 28 after CTX injury clearly demonstrated
437 the essential role of DUSP13 and DUSP27 in muscle regeneration (Figure 4A–4D). Specifically, seven

438 days post-injury, we observed a notable increase in PAX7 (+) cells and a decrease in MYOGENIN
439 (+) cells (Figure 4E, 4F, 4H, and 4I) in DKO muscles compared to those in WT mice. Furthermore,
440 the percentage of Ki67 (+) cells in MYOGENIN (+) cells was increased significantly in DKO muscles
441 (Figure 4G and 4J). At 28 days post-injury, when MuSCs are returning to their niche after completing
442 the muscle regeneration process, we observed a trend towards a reduction in the number of PAX7 (+)
443 cells (Figure S4J and S4K), accompanied by a notable increase in the number of perduring
444 MYOGENIN (+) cells undergoing regeneration (Figure S4L and S4M).
445 To confirm our *in vivo* findings indicating a severe delay in muscle regeneration in DKO mice, we
446 isolated MuSCs from DKO and WT mice using magnetic cell sorting (MACS) with α7-integrin
447 microbeads [6,23] and cultured them for three days. Immunofluorescent analysis using antibodies
448 against PAX7 and MYOD showed a lower proportion of PAX7 (-) and MYOD (+) cells and an
449 increased number of PAX7 (+) and MYOD (+) cells in the DKO mice (Figure 4K–4M), indicating
450 that DUSP13/DUSP27 are necessary for the transition from proliferation to differentiation during
451 myogenesis. In addition, we observed a higher number of proliferating Ki67 (+) MuSCs in DKO mice
452 (Figure S5A–S5C). In addition, both myotube width and fusion index exhibited a significant reduction
453 in DKO mice relative to in WT mice after six days of MuSC differentiation (Figure 4N–4P). The
454 findings suggest that DUSP13 and DUSP27 dictate the balance between the proliferation and
455 differentiation of MuSCs during myogenesis.
456
457 ***Single-cell RNA sequencing revealed that Dusp13 and Dusp27 are highly expressed in the late***
458 ***differentiation stage of MuSCs.***
459 While MYOD activates *Dusp13* and *Dusp27* through their E-box, and *DKO* mice exhibit diminished
460 muscle regeneration activity, the molecular mechanisms by which DUSP13 and DUSP27 regulate
461 myogenesis remain elusive. Additionally, the expression patterns of *Dusp13* and *Dusp27* in different
462 stages of myogenic progenitors within the highly heterogeneous MuSC populations are not well-
463 defined. To gain a more comprehensive understanding of the molecular signatures of *Dusp13* and
464 *Dusp27*-expressing myogenic cells, we conducted single-cell RNA sequencing (scRNA-seq) on
465 MyoD-high expressing cells isolated from cultured MuSCs obtained from MyoD-KI mice (Figure 5A).
466 The approach allowed us to enrich activated/differentiated MyoD (+) cells [23]. MuSCs from MyoD-
467 KI mice were cultured for five days in a growth medium, and only live MyoD-high MuSCs with PI
468 (-) negative populations were sorted by fluorescence-activated cell sorter (FACS) for subsequent
469 scRNA-seq library preparation (Figure 5A). Utilizing the Seurat single-cell analysis package, we
470 identified five distinct clusters of cells (C0–C4) presented in the uniform manifold approximation and
471 projection (UMAP) (Figure 5B). Each cluster exhibited a unique transcriptomic fingerprint
472 characterized by the top 10 differentially expressed genes (Figure S6A).

To further understand the characteristics of the clusters, a Gene Ontology (GO) analysis on differentially expressed genes (DEGs) was conducted among the clusters (Figure S6B–S6F). C0 and C4 showed upregulation of genes associated with chromosome segregation and DNA replication (Figure S6B and S6F). C1 and C3 displayed strong enrichment for terms related to muscle differentiation, maturation, and contraction (Figure S6C and S6E). C2 was characterized by genes associated with ameboidal-type cell migration and extracellular organization (Figure S6D), akin to the previously reported MyoD-low MuSC signatures [23]. Next, we investigated cell cycle and myogenic markers, including *MKi67, E2f1, Ccnd1, Ccnd3, Pax7, Myf5, Myod1, Myogenin, Cdkn1c (p21), Myh3, Dusp13*, *and Dusup27* on UMAP (Figure 5C). *MyoD* is expressed ubiquitously across all clusters but with variations between the clusters (Figure 5C). *Mki67* and *E2f1*, which are proliferative markers, were highly expressed in C0 and C4 but not in C1, C2, and C3 (Figure 5C). Undifferentiated MuSC markers, *Pax7* and *Myf5*, were enriched exclusively in C0 and C2 (Figure 5C). Notably, *Dusp13* and *Dusp27* exhibited pronounced enrichment in C1 and C3, characterized by upregulation of genes associated with myogenic differentiation and maturation (Figure 5C). Considering the GO term and UMAP, C0 and C4 represent proliferative states, while C1 and C3 contain the differentiation and maturation state of MuSCs. Conversely, C2 reflects the self-renewing MuSCs returning to the undifferentiated state.

Furthermore, we used Monocle to analyze the MYOD-high expressing MuSC clusters and infer MuSC state trajectories (Figure 5D–5F). The cell state trajectory model revealed three branches for the MyoD-high-expressing MuSCs. The branches suggested that some clusters were transitioning toward further proliferation (C1, C4), myogenic differentiation/maturation (C1, C3), or self-renewal (C2) to return to an undifferentiated quiescent state (Figure 5D). Subsequently, we focused the Monocle analysis on selected genes related to myogenic development/regeneration and cell cycle (*Pax7, Myf5, Myod1, Myogenin, Myf6, Myh3, Myh4, Hes6, Acta1, ccnd1, ccnd3, E2f1, Mki67, Cdkn1c [p21], Dusp13, and Dusp27*). Cluster 3 contained *Dusp13* and *Dusp27*, along with *Myogenin, Myh3, Hes6, Acta1,* and *Cdkn1c (p21)* (Figure 5E and 5F). When visualizing the pseudotime progression axis of these selected genes, we observed that cells from C0 and C4, which expressed genes associated with the cell cycle (*Mki67* and *E2f1*) but had lower expression of *Pax7* and *Myf5*, were located at the initiation point of pseudotime (Figure 5E and 5F). Cells from C2, which showed lower levels of *Mki67* and *E2f1* but higher levels of *Pax7*, *Myf5*, and *Ccnd1*, were found mainly in the middle point of pseudotime, suggesting that C2 represents a self-renewing MuSCs state [23,44]. In contrast, cells from C1 and C3, which highly expressed genes associated with myogenic differentiation and maturation, were located distally at the endpoint of pseudotime (Figure 5E and 5F), indicating myogenic differentiation and maturation states (Figure 5E and 5F). *Dusp13* and *Dusp27*, enriched in C1 and C3, progressed alongside myogenic differentiation markers and *Cdkn1c (p21)* (Figure 5E and 5F). To further support our scRNA-seq data, we visualized *Dusp13* and *Dusp27* RNA in different stages of

509 myogenic cells (freshly isolate, GM6, and DM6) using RNAscope (Figure S7A and S7B). The results
510 revealed that puncta for both genes were either not visible or present in low numbers in the freshly
511 isolated PAX7+ MuSCs but increased gradually as myogenesis progressed (Figure S7A and S7B).
512 Overall, clustering and cell state trajectory analysis based on scRNA-seq data of MyoD-high-
513 expressing MuSCs and the RNAscope analysis suggest that *Dusp13* and *Dusp27* are enriched only in
514 the late stages of MyoD-positive MuSCs co-expressing *Myogenin*, *Myh3*, and *Cdkn1c*. This indicates
515 that these genes may regulate the transition from a proliferative state to a myogenic differentiation
516 state.
517
518 ***Dusp13 drives precocious muscle differentiation* in MuSCs.**
519 Since our scRNA-seq analysis of MyoD-high expressing cells indicates that *Dusp13* and *Dusp27* are
520 expressed in the subset of cells expressing late myogenic markers, such as myogenin, to investigate
521 whether DUSP13 plays a role in initiating the differentiation process during myogenesis, we
522 transduced FACS-isolated MuSCs from adult Pax7-YFP mice with an adenovirus vector expressing
523 *Dusp13* or GFP under the CMV promoter (Figure 6A, Figure S8A, and S8B). Two days post-infection,
524 we observed a significant reduction in the number of MuSCs transduced with *Dusp13* compared to
525 the GFP control (Figure 6B). Notably, immunofluorescent analysis using antibodies against PAX7
526 and MYOGENIN showed that *Dusp13* overexpression led to induction of MYOGENIN expression in
527 PAX7 (+) cells, which are typically not detected under normal culture conditions (Figure 6C and 6D).
528 However, overexpression of *Dusp13* did not alter MyoD expression (Figure S8C and S8D).
529 Furthermore, when we cultured MuSCs overexpressing *Dusp13* for seven days and assessed their
530 myotube formation ability, we found that both the myotube width and fusion index were lower
531 compared to the GFP control (Figure 6E–6H). These results suggest that overexpression of *Dusp13* in
532 activated MuSCs induces precocious differentiation, which inhibits the amplification of MuSCs and
533 results in smaller myotube size and lower fusion index.
534 To investigate whether the phosphatase activity of DUSP13 is involved in myogenic induction, we
535 transduced MuSCs from adult PAX7-YFP mice with pAd-Dusp13_Mut, which lacks enzymatic
536 activity. Surprisingly, we discovered that DUSP13 without phosphatase activity still enhanced the
537 population of PAX7 (+) and MYOGENIN (+) cells to the same extent as normal DUSP13 (Figure S8E
538 and S8F). Overall, the results suggest that DUSP13 acts as a driver for myogenin during myogenic
539 progression, which is mediated by phosphatase activity-independent mechanisms.
540
541 **Discussion**
542 Skeletal muscle regeneration relies heavily on the activity of muscle stem cells (MuSCs). The
543 regulation of MuSC dynamics is mediated by the sequential expression of various transcription factors
544 during myogenesis. MYOD is essential for myogenic lineage specification during embryogenesis

545 [12,45,46]. In adult mice regeneration, MYOD is induced in activated MuSCs, modulating the balance
546 between self-renewal and differentiation [21,22,47–49]. However, the molecular mechanisms by
547 which MYOD governs fate determination in MuSCs remain unclear, particularly regarding its direct
548 targets beyond *Myogenin*, which have not been fully identified. Therefore, it is crucial to identify
549 additional direct targets of MYOD that play key roles in skeletal myogenesis during development and
550 regeneration. The diverse and highly heterogeneous nature of MuSCs, particularly during myogenesis,
551 has posed a challenge in deciphering molecular signatures in MYOD-expressing MuSCs due to a lack
552 of appropriate tools. This has hindered the elucidation of MYOD's role in fate determination. To
553 address this, we previously engineered MyoD-KI mice, providing a platform to distinguish and isolate
554 undifferentiated (MyoD-low) and committed MuSCs (MyoD-high).

555 In the present study, we integrated our previously established whole-transcriptome data
556 encompassing quiescent, undifferentiated (MyoD-low), and committed (MyoD-high) MuSCs from
557 MyoD-KI reporter mice [23] with publicly available databases from *MyoD* KO mice [40], Chip-atlas
558 [41,42], and *MyoD* overexpression [43]. Through this integration, we identified *Dusp13* as a novel
559 molecular switch regulated by MyoD, stimulating the initiation of myogenic differentiation. To
560 understand the function of DUSP13, we generated *Dusp13* KO mice using CRISPR-Cas9.
561 Surprisingly, muscle development and regeneration abilities in *Dusp13* KO mice mirrored those of
562 their WT counterparts. This led us to investigate the compensatory role of other members of the DUSP
563 family. We found that *Dusp27* was also directly regulated by MyoD. Although *Dusp27* KO mice
564 generated in the present study did not exhibit marked differences in muscle development and
565 regenerative ability following CTX injury, the combined deficiency of *Dusp13* and *Dusp27* in mice
566 resulted in substantial delays in muscle regeneration after CTX injury. The findings suggest a
567 compensatory interplay between DUSP13 and DUSP27 during muscle regeneration. The quantities of
568 PAX7 (+) quiescent MuSCs were identical between WT and DKO mice before injury. However, at
569 28 days post-CTX injury, when muscle regeneration was almost complete, DKO mice had lower levels
570 of PAX7 (+) cells compared to WT mice. Conversely, DKO mice had more MYOGENIN (+) cells
571 remaining at day 28 post-injury compared to WT mice. At day 7 post-injury, DKO mice had higher
572 numbers of PAX7 (+) cells and fewer MYOGENIN (+) cells. The results suggest that the absence of
573 *Dusp13* and *Dusp27* promotes the imbalance of the fate determination processes in MuSCs following
574 muscle injury. *In vitro* analyses employing isolated MuSCs from DKO mice supported these findings,
575 showing that the absence of *Dusp13* and *Dusp27* promotes proliferation rather than differentiation.
576 Consequently, the delay/failure in transitioning from the proliferation phases to differentiation,
577 attributed to the deficiency of *Dusp13* and *Dusp27*, disrupts the muscle repair process in adult mice.

578 To further investigate the regulatory dynamics of *Dusp13* and *Dusp27* in fate determination, we
579 conducted scRNA-seq on MyoD-high expressing MuSCs isolated from MyoD-KI mice. Intriguingly,
580 both *Dusp13* and *Dusp27* expression were enriched in specific clusters (C1 and C3) within the MyoD-

high expressing MuSC populations. The clusters were characterized by increased expression of late myogenic markers, such as *Myogenin, Myh3,* and *Cdkn1a*, and decreased expression of *Pax7*, *MKi67*, and *Myf5*. Pseudotime cell state trajectory analysis was used to distinguish the fate determination of MuSCs during myogenesis. Cluster C0 represented a proliferative state with high expression of undifferentiated markers (*Pax7* and *Myf5*) and cell cycle markers (*MKi67* and *E2f1*), which are projected to further proliferate (C4), differentiate/mature (C1 and C3), or self-renew to return to an undifferentiated quiescent state (C2). We believe that the scRNA-seq data from our MyoD-KI mice will provide a valuable resource for uncovering novel molecular mechanisms involved in myogenic fate transition (proliferation, differentiation, or self-renewal/quiescence) of activated MuSCs during myogenesis.

Considering the limited expression of *Dusp13* and *Dusp27* in C1 and C3 (diifferentiate/mature clusters), we hypothesized that the two genes play a crucial role in the transition from proliferation to differentiation. In our study, we overexpressed *Dusp13* in activated MuSCs *in vitro* using an adenovirus vector. Although the expression of PAX7 and MYOGENIN is typically mutually exclusive during myogenesis [50], a small subset of cells exhibits positivity for both PAX7 and MYOGENIN, representing an intermediate population initiating differentiation [51]. In our model, a limited number of PAX7 (+) and MYOGENIN (+) cells were also identified. Notably, *Dusp13* overexpression augmented the populations of PAX7 (+) and MYOGENIN (+) cells significantly. Moreover, the promoter activities of both Dusp13 and Dusp27 were not upregulated by the *Myogenin* expression vector. The results collectively corroborate the findings of our scRNA-seq analysis, supporting the hypothesis that the MYOD-DUSP13/DUSP27-MYOGENIN regulatory networks also orchestrate the initiation of differentiation during muscle regeneration in adult mice.

There are limited studies on the regulatory roles of the DUSP family in myogenesis, leaving the molecular targets modulated by DUSP13 and DUSP27 in MuSCs currently unknown. The DUSPs family possesses the dual ability to dephosphorylate phosphor-serine/threonine and phospho-tryosoine residues. Currently, 25 different DUSPs are identified and categorized into six subfamilies [25]. Our single-cell RNA-seq analysis of MyoD-high MuSCs revealed enrichment of other DUSP family members such as *Dusp3* and *Dusp14* in C1 and C3 clusters (data not shown). While the relationship with Dusp13/27 was not investigated in this study, it is noteworthy that the expressions of *Dusp3* and *Dusp14* were not compensatory upregulated by the loss of *Dusp13* and *Dusp27*, suggesting that uncovering additional functions of other DUSP family members in myogenesis is warranted in future research.

DUSP13, an atypical DUSP, has versatile dephosphorylation substrates, including mitogen-activated protein kinases (MAPKs). Forced expression of pAd-Dusp13_Mut vector, which has no phosphatase activity, into MuSCs, led to the emergence of PAX7 (+) and MYOGENIN (+) cells *in vitro*, indicating phosphatase-independent mechanisms mediated by DUSP13 for myogenic

differentiation. Interestingly, DUSP27 is recognized as a pseudo-phosphatase, characterized by catalytically inactive phosphatase activity. Various pseudo-phosphatases are reported to possess pivotal functions in different organisms and pathological conditions [33]. Inhibition of ERK1/2 promotes myogenic differentiation and fusion in both mice and avian models [52]. The DUSP family, lacking a kinetic-interacting motif, inhibits ERK1/2 signaling [53–55], suggesting that the phosphatase-independent activities of DUSP13 and DUSP27 potentially regulate ERK signaling in MuSCs. Future investigations are expected to unravel the detailed molecular mechanisms by which DUSP13 and DUSP27 orchestrate fate switching in activated MuSCs during myogenesis.

Although our study demonstrates that DKO mice exhibit reduced muscle regeneration capacity, several limitations must be considered when interpreting our results. The systemic deletion of *Dusp13* and *Dusp27* complicates the isolation of specific effects on muscle regeneration. To further investigate this, we isolated MuSCs from DKO mice and found impaired myotube formation compared to WT mice. However, optimal muscle regeneration requires the coordinated interaction of multiple cell types, including inflammatory cells [56,57] and fibro-adipogenic progenitors (FAPs) [58,59]. The expression of *Dusp13* and *Dusp27* is comparatively lower in other tissues than in skeletal muscles (Figure S2A–S2B). Furthermore, re-analysis of single-cell and -nucleus RNA-seq data from intact skeletal muscle indicates that *Dusp13* and *Dusp27* are highly enriched in myonuclei but not in other cell types, such as immune cells and endothelial cells [60]. Most FAPs are negative for *Dusp13* and *Dusp27*, although a small subset expresses the genes. Given the crucial role of FAPs in muscle regeneration [58,59,61], we cannot entirely exclude the possibility that the delayed muscle regeneration in DKO mice could partially result from the loss of *Dusp13* and *Dusp27* in the subset of FAPs. The area of infiltrated macrophages was not apparent between WT and DKO muscles post-injury (data not shown). Further investigations using $Pax7^{CreERT2}$ mice to specifically deplete *Dusp13* and *Dusp27* in MuSCs will be necessary to clarify this aspect. Another unresolved issue is why DKO mice exhibit no differences in skeletal muscle size, weight, or histology compared to WT mice under normal conditions. The lack of effect from the loss of DUSP13 and DUSP27 on muscle development during embryogenesis is unclear. It is possible that other DUSP family members compensate for their roles during embryonic and postnatal muscle formation, or that the downstream targets of DUSP13 and DUSP27 differ between muscle regeneration and embryonic myogenesis.

In summary, using our previously established MyoD-KI mice model, we identified *Dusp13* and *Dusp27* as novel MYOD target genes that play a pivotal role in the fate switching of MuSCs. Furthermore, we demonstrated that *Dusp13* and *Dusp27* expressions are highly enriched in differentiation clusters revealed by scRNA-seq of MyoD-high expressing MuSCs. Beyond *Dusp13* and *Dusp27* being novel determinants for the initiation of myogenic differentiation, further analysis of scRNA-seq data within each cluster would yield valuable insights into potential targets of DUSP13 or DUSP27 in MuSCs during myogenesis.

Acknowledgments

We would like to thank Satoshi Yamazaki and Yuji Yamazaki from the Division of Stem Cell Therapy, University of Tsukuba, for their valuable technical assistance in cell sorting using flow cytometry. We also thank Hiroshi Sakai (Ehime University) for his support in the RNAscope analysis and Shin Fujimaki (Kumamoto University) for helping with single-cell and -nucleolus RNA-seq analysis of their data. This work was supported by grants from the MEXT Leading Initiative for Excellent Young Researchers (R.F.), Grant-in-Aid for Early-Career Scientists (21K17679; R.F.), and Grant-in-Aid for Scientific Research (B) (24K02876; R.F.) from the Japan Society for the Promotion of Science (JSPS). This research was also supported by AMED-CREST (JP23gm171008h). This work was also supported, in part, by grants to R.F. from the Takeda Science Foundation and Mochida Memorial Foundation for Medical and Pharmaceutical Research. Furthermore, this work received support from the Grant-in-Aid for the Japan Aerospace Exploration Agency (14YPTK-407 005512; S.T.) and the Grant-in-Aid for Scientific Research on Innovative Area from MEXT (18H04965; S.T.). T.H. and S.S were funded by JSPS Research Fellowships for Young Scientists (22J10954 [T.H.] and 23KJ0287 [S.S.]).

Competing interests

The authors declare no competing financial interests.

Author contributions

T.H., S.M., S.T., and R.F. conceived the study and designed the experiments. T.H., S.S., R.T., R.O., S.F., M.K., A.N., Y.O., M.M., S.M., D.S., E.W., T.K., and R.F. performed the experiments and bioinformatics analysis. T.H., G.W., T.S., and R.F. performed single-cell RNA-seq analysis. T.H., S.T., and R.F. wrote the manuscript. All authors contributed to the analysis and interpretation of results and reviewed the manuscript.

Data Availability Statement

- All unique reagents generated in this study are available from the corresponding author, Ryo Fujita (fujiryo@md.tsukuba.ac.jp), in accordance with the relevant material transfer agreements.
- Single-cell RNA-seq data have been deposited in the NCBI Gene Expression Omnibus (GEO) and can be accessed with GSE250228.
- This paper does not report original code.
- Any additional information required to reanalyze the data reported in this paper is available from the corresponding author, Ryo Fujita (fujiryo@md.tsukuba.ac.jp) upon request.

Additional information

Supplementary Information is available for this paper.

691 **References**

692 1 Mauro A. Satellite cell of skeletal muscle fibers. J Biophys Biochem Cytol
693 1961;9:493–495.
694 2 Murphy MM, Lawson JA, Mathew SJ, et al. Satellite cells, connective tissue
695 fibroblasts and their interactions are crucial for muscle regeneration. Development
696 2011;138:3625–3637.
697 3 Collins CA, Olsen I, Zammit PS, et al. Stem cell function, self-renewal, and
698 behavioral heterogeneity of cells from the adult muscle satellite cell niche. Cell
699 2005;122:289–301.
700 4 van Velthoven CTJ, Rando TA. Stem Cell Quiescence: Dynamism, Restraint,
701 and Cellular Idling. Cell Stem Cell 2019;24:213–225.
702 5 Kuang S, Kuroda K, Le Grand F, et al. Asymmetric self-renewal and
703 commitment of satellite stem cells in muscle. Cell 2007;129:999–1010.
704 6 Sénéchal C, Fujita R, Jamet S, et al. The adhesion G-protein-coupled receptor
705 Gpr116 is essential to maintain the skeletal muscle stem cell pool. Cell Reports
706 2022;41:111645.
707 7 Zammit PS, Partridge TA, Yablonka-Reuveni Z. The Skeletal Muscle Satellite
708 Cell: The Stem Cell That Came in From the Cold. J Histochem Cytochem
709 2006;54:1177–1191.
710 8 Relaix F, Rocancourt D, Mansouri A, et al. A Pax3/Pax7-dependent population
711 of skeletal muscle progenitor cells. Nature 2005;435:948–953.
712 9 Seale P, Sabourin LA, Girgis-Gabardo A, et al. Pax7 Is Required for the
713 Specification of Myogenic Satellite Cells. Cell 2000;102:777–786.
714 10 Relaix F, Montarras D, Zaffran S, et al. Pax3 and Pax7 have distinct and
715 overlapping functions in adult muscle progenitor cells. Journal of Cell Biology
716 2006;172:91–102.
717 11 Oustanina S, Hause G, Braun T. Pax7 directs postnatal renewal and
718 propagation of myogenic satellite cells but not their specification. EMBO J
719 2004;23:3430–3439.
720 12 Rudnicki MA, Schnegelsberg PNJ, Stead RH, et al. MyoD or Myf-5 is required
721 for the formation of skeletal muscle. Cell 1993;75:1351–1359.
722 13 Yamamoto M, Legendre NP, Biswas AA, et al. Loss of MyoD and Myf5 in
723 Skeletal Muscle Stem Cells Results in Altered Myogenic Programming and Failed
724 Regeneration. Stem Cell Reports 2018;10:956–969.
725 14 Kassar-Duchossoy L, Gayraud-Morel B, Gomès D, et al. Mrf4 determines
726 skeletal muscle identity in Myf5:Myod double-mutant mice. Nature 2004;431:466–471.

727 15 Nabeshima Y, Hanaoka K, Hayasaka M, et al. Myogenin gene disruption
728 results in perinatal lethality because of severe muscle defect. Nature 1993;364:532–535.
729 16 Zismanov V, Chichkov V, Colangelo V, et al. Phosphorylation of eIF2α Is a
730 Translational Control Mechanism Regulating Muscle Stem Cell Quiescence and Self-
731 Renewal. Cell Stem Cell 2016;18:79–90.
732 17 Crist CG, Montarras D, Buckingham M. Muscle satellite cells are primed for
733 myogenesis but maintain quiescence with sequestration of Myf5 mRNA targeted by
734 microRNA-31 in mRNP granules. Cell Stem Cell 2012;11:118–126.
735 18 Fujita R, Zismanov V, Jacob J-M, et al. Fragile X mental retardation protein
736 regulates skeletal muscle stem cell activity by regulating the stability of Myf5 mRNA.
737 Skeletal Muscle 2017;7:18.
738 19 Hausburg MA, Doles JD, Clement SL, et al. Post-transcriptional regulation of
739 satellite cell quiescence by TTP-mediated mRNA decay. eLife 2015;4:e03390.
740 20 de Morrée A, van Velthoven CTJ, Gan Q, et al. Staufen1 inhibits MyoD
741 translation to actively maintain muscle stem cell quiescence. Proc Natl Acad Sci USA
742 2017;114:E8996–E9005.
743 21 Megeney LA, Kablar B, Garrett K, et al. MyoD is required for myogenic stem
744 cell function in adult skeletal muscle. Genes Dev 1996;10:1173–1183.
745 22 Yablonka-Reuveni Z, Rudnicki MA, Rivera AJ, et al. The Transition from
746 Proliferation to Differentiation Is Delayed in Satellite Cells from Mice Lacking MyoD.
747 Developmental Biology 1999;210:440–455.
748 23 Fujita R, Mizuno S, Sadahiro T, et al. Generation of a MyoD knock-in reporter
749 mouse line to study muscle stem cell dynamics and heterogeneity. iScience
750 2023;26:106592.
751 24 Kitajima Y, Ono Y. Visualization of PAX7 protein dynamics in muscle
752 satellite cells in a YFP knock-in-mouse line. Skelet Muscle 2018;8:26.
753 25 Alonso A, Pulido R. The extended human PTPome: a growing tyrosine
754 phosphatase family. FEBS J 2016;283:1404–1429.
755 26 Denu JM, Dixon JE. A catalytic mechanism for the dual-specific phosphatases.
756 Proc Natl Acad Sci U S A 1995;92:5910–5914.
757 27 Denu JM, Dixon JE. Protein tyrosine phosphatases: mechanisms of catalysis
758 and regulation. Curr Opin Chem Biol 1998;2:633–641.
759 28 Bermudez O, Pagès G, Gimond C. The dual-specificity MAP kinase
760 phosphatases: critical roles in development and cancer. Am J Physiol Cell Physiol
761 2010;299:C189-202.

762 29 Patterson KI, Brummer T, O'Brien PM, et al. Dual-specificity phosphatases:
763 critical regulators with diverse cellular targets. Biochem J 2009;418:475–489.
764 30 Tonks NK. Protein tyrosine phosphatases: from genes, to function, to disease.
765 Nat Rev Mol Cell Biol 2006;7:833–846.
766 31 Aoki N, Aoyama K, Nagata M, et al. A growing family of dual specificity
767 phosphatases with low molecular masses. J Biochem 2001;130:133–140.
768 32 Huang C-Y, Tan T-H. DUSPs, to MAP kinases and beyond. Cell Biosci
769 2012;2:24.
770 33 Reiterer V, Pawłowski K, Desrochers G, et al. The dead phosphatases society:
771 a review of the emerging roles of pseudophosphatases. FEBS J 2020;287:4198–4220.
772 34 Fero K, Bergeron SA, Horstick EJ, et al. Impaired embryonic motility in
773 dusp27 mutants reveals a developmental defect in myofibril structure. Dis Model Mech
774 2014;7:289–298.
775 35 Boyer JG, Prasad V, Song T, et al. ERK1/2 signaling induces skeletal muscle
776 slow fiber-type switching and reduces muscular dystrophy disease severity. JCI Insight
777 2019;4:e127356.
778 36 Chen H-H, Luche R, Wei B, et al. Characterization of two distinct dual
779 specificity phosphatases encoded in alternative open reading frames of a single gene
780 located on human chromosome 10q22.2. J Biol Chem 2004;279:41404–41413.
781 37 Alonso A, Sasin J, Bottini N, et al. Protein tyrosine phosphatases in the human
782 genome. Cell 2004;117:699–711.
783 38 Fujita R, Jamet S, Lean G, et al. Satellite cell expansion is mediated by P-eIF2α
784 dependent *Tacc3* translation. Development 2020:dev.194480.
785 39 Grant CE, Bailey TL, Noble WS. FIMO: scanning for occurrences of a given
786 motif. Bioinformatics 2011;27:1017–1018.
787 40 Wang R, Chen F, Chen Q, et al. MyoD is a 3D genome structure organizer for
788 muscle cell identity. Nat Commun 2022;13:205.
789 41 Oki S, Ohta T, Shioi G, et al. ChIP-Atlas: a data-mining suite powered by full
790 integration of public ChIP-seq data. EMBO Rep 2018;19:e46255.
791 42 Zou Z, Ohta T, Miura F, et al. ChIP-Atlas 2021 update: a data-mining suite for
792 exploring epigenomic landscapes by fully integrating ChIP-seq, ATAC-seq and
793 Bisulfite-seq data. Nucleic Acids Res 2022;50:W175–W182.
794 43 Conerly ML, Yao Z, Zhong JW, et al. Distinct Activities of Myf5 and MyoD
795 Indicate Separate Roles in Skeletal Muscle Lineage Specification and Differentiation.
796 Dev Cell 2016;36:375–385.

797 44 Brett JO, Arjona M, Ikeda M, et al. Exercise rejuvenates quiescent skeletal
798 muscle stem cells in old mice through restoration of Cyclin D1. Nat Metab 2020;2:307–
799 317.
800 45 Davis RL, Weintraub H, Lassar AB. Expression of a single transfected cDNA
801 converts fibroblasts to myoblasts. Cell 1987;51:987–1000.
802 46 Rudnicki MA, Braun T, Hinuma S, et al. Inactivation of MyoD in mice leads to
803 up-regulation of the myogenic HLH gene Myf-5 and results in apparently normal
804 muscle development. Cell 1992;71:383–390.
805 47 Sabourin LA, Girgis-Gabardo A, Seale P, et al. Reduced Differentiation
806 Potential of Primary MyoD−/− Myogenic Cells Derived from Adult Skeletal Muscle.
807 Journal of Cell Biology 1999;144:631–643.
808 48 White JD, Scaffidi A, Davies M, et al. Myotube formation is delayed but not
809 prevented in MyoD-deficient skeletal muscle: studies in regenerating whole muscle
810 grafts of adult mice. J Histochem Cytochem 2000;48:1531–1544.
811 49 Wood WM, Etemad S, Yamamoto M, et al. MyoD-expressing progenitors are
812 essential for skeletal myogenesis and satellite cell development. Developmental Biology
813 2013;384:114–127.
814 50 Olguin HC, Yang Z, Tapscott SJ, et al. Reciprocal inhibition between Pax7 and
815 muscle regulatory factors modulates myogenic cell fate determination. J Cell Biol
816 2007;177:769–779.
817 51 Halevy O, Piestun Y, Allouh MZ, et al. Pattern of Pax7 expression during
818 myogenesis in the posthatch chicken establishes a model for satellite cell differentiation
819 and renewal. Developmental Dynamics 2004;231:489–502.
820 52 Eigler T, Zarfati G, Amzallag E, et al. ERK1/2 inhibition promotes robust
821 myotube growth via CaMKII activation resulting in myoblast-to-myotube fusion.
822 Developmental Cell 2021;56:3349-3363.e6.
823 53 Hu Y, Mivechi NF. Association and regulation of heat shock transcription
824 factor 4b with both extracellular signal-regulated kinase mitogen-activated protein
825 kinase and dual-specificity tyrosine phosphatase DUSP26. Mol Cell Biol
826 2006;26:3282–3294.
827 54 Huang K, Serria MS, Nakabayashi H, et al. Molecular cloning and functional
828 characterization of the mouse mafB gene. Gene 2000;242:419–426.
829 55 Marti F, Krause A, Post NH, et al. Negative-feedback regulation of CD28
830 costimulation by a novel mitogen-activated protein kinase phosphatase, MKP6. J
831 Immunol 2001;166:197–206.

832 56 Arnold L, Henry A, Poron F, et al. Inflammatory monocytes recruited after
833 skeletal muscle injury switch into antiinflammatory macrophages to support
834 myogenesis. Journal of Experimental Medicine 2007;204:1057–1069.
835 57 Fujita R, Kawano F, Ohira T, et al. Anti-interleukin-6 receptor antibody
836 (MR16-1) promotes muscle regeneration via modulation of gene expressions in
837 infiltrated macrophages. Biochimica et Biophysica Acta (BBA) - General Subjects
838 2014;1840:3170–3180.
839 58 Joe AWB, Yi L, Natarajan A, et al. Muscle injury activates resident
840 fibro/adipogenic progenitors that facilitate myogenesis. Nat Cell Biol 2010;12:153–163.
841 59 Uezumi A, Fukada S, Yamamoto N, et al. Mesenchymal progenitors distinct
842 from satellite cells contribute to ectopic fat cell formation in skeletal muscle. Nat Cell
843 Biol 2010;12:143–152.
844 60 Fujimaki S, Matsumoto T, Muramatsu M, et al. The endothelial Dll4–muscular
845 Notch2 axis regulates skeletal muscle mass. Nat Metab 2022;4:180–189.
846 61 Lukjanenko L, Karaz S, Stuelsatz P, et al. Aging Disrupts Muscle Stem Cell
847 Function by Impairing Matricellular WISP1 Secretion from Fibro-Adipogenic
848 Progenitors. Cell Stem Cell 2019;24:433-446.e7.
849
850

851 **Figures**

Figure 1 (Hayashi et al.)

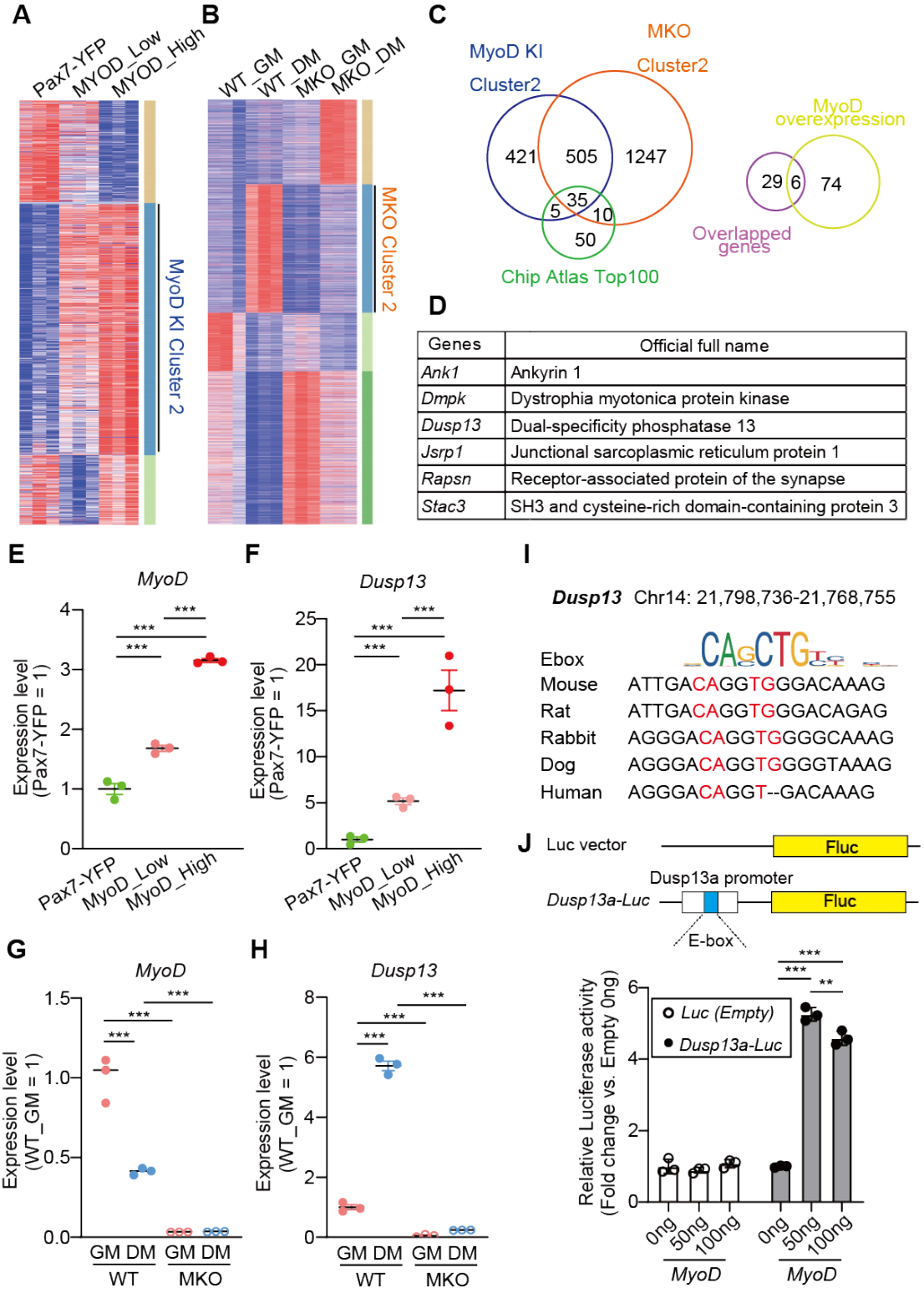

Genes	Official full name
Ank1	Ankyrin 1
Dmpk	Dystrophia myotonica protein kinase
Dusp13	Dual-specificity phosphatase 13
Jsrp1	Junctional sarcoplasmic reticulum protein 1
Rapsn	Receptor-associated protein of the synapse
Stac3	SH3 and cysteine-rich domain-containing protein 3

852

853

854 **Figure 1. *Dusp13* is a novel target regulated by MyoD.**

855 **(A)** Clustering heatmap showing differentially expressed genes in RNA-seq data from Pax7-YFP
856 (Quiescent MuSCs; QSCs), MyoD-low (MyoD-tdTomato low), and MyoD-high (MyoD-tdTomato
857 high) (n = 3 per group).

858 **(B)** Clustering heatmap of differentially expressed genes in RNA-seq between wild-type (WT**)** growth
859 medium (GM) (WT_GM), *MyoD* knock-out GM (MKO_GM), WT differentiation medium (WT_DM),
860 and MKO_DM (n = 3 per group).

861 **(C)** Venn diagrams of indicated clusters from (**A, B)** and ChIP atlas top 100 genes potentially regulated
862 by *MyoD* (Left). Venn diagrams of overlapped 35 genes (left) and 80 genes upregulated by *MyoD*
863 overexpression in MEFs (Right).

864 **(D)** List of six genes from (**C**).

865 **(E, F)** Gene expression of *MyoD* (**E**) or *Dusp13* (**F**) analyzed by RNA-seq in the Pax7-YFP, MyoD-
866 low, and MyoD-high MuSCs (n = 3 per group).

867 **(G, H)** Gene expression of *MyoD* (**G**) or *Dusp13* (**H**) analyzed by RNA-seq in the WT_GM, WT_DM,
868 MKO_GM, and MKO_DM groups (n = 3 per group).

869 **(I)** E box-like sequences in the promoter region of *Dusp13* in mammalian species.

870 **(J)** Luciferase reporter constructs of *Dusp13* upstream region (−150 to +50) containing an E box-like
871 sequence (Top). Relative *Dusp13*-luciferase reporter activities in HEK293T cells overexpressing
872 *MyoD* (Bottom) (n = 3 per group).

873 All data are presented as mean ± standard error of the mean (SEM)

874 P values calculated using edge R **(E, F)** (FDR-corrected), DEseq2 **(G, H)** (FDR-corrected), or Tukey's
875 test **(J)**; **P < 0.01, ***P < 0.001, n.s., not significant.

876

877

Figure 2 (Hayashi et al.)

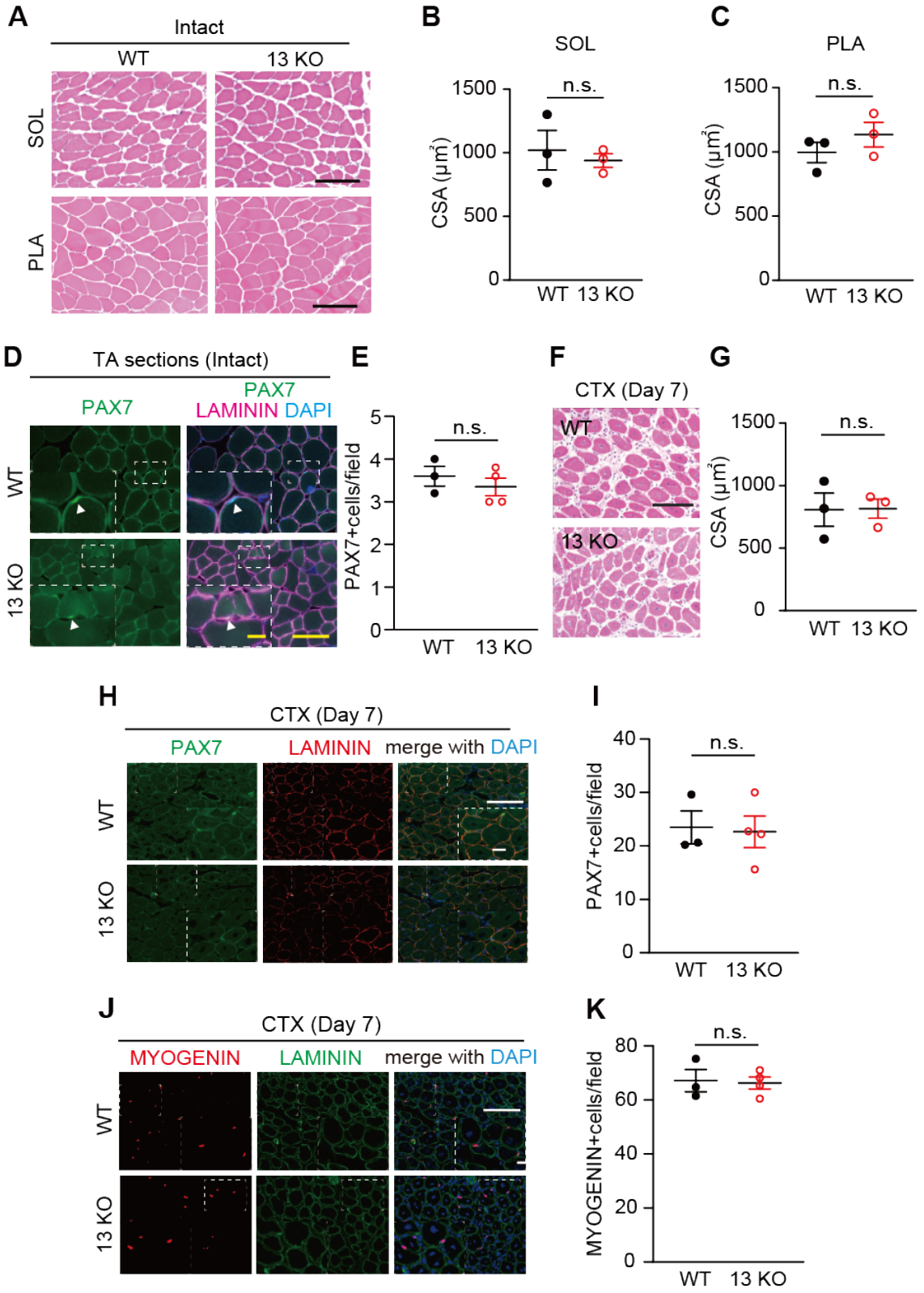

878

879 **Figure 2. Absence of skeletal muscle phenotype in *Dusp13* knock-out (13 KO) mice during**
880 **development and regeneration.**
881 **(A)** Hematoxylin and eosin (H&E) staining of Soleus (SOL) and Plantaris (PLA) muscle cross-
882 sections of male *Dusp13* knock-out (13 KO) and WT mice at 10 weeks. Scale bar: 100 µm.
883 **(B, C)** Cross-sectional area (CSA) of SOL (B) or PLA (C) (n = 3 per group).
884 **(D)** Immunofluorescence of PAX7 and LAMININ in intact TA muscles. Scale bar: 100 µm. The area
885 in the white dotted boxes is shown at a higher magnification. Scale bar: 25 µm.
886 **(E)** Average number of PAX7 (+) nuclei in DAPI (+) in **(D)**.
887 **(F)** H&E staining of tibialis anterior (TA) muscle cross-sections of male 13 KO and WT mice at 12
888 weeks, 7 days post cardiotoxin (CTX) injury. Scale bar: 100 µm.
889 **(G)** CSA of damaged TA muscles (n = 3 per group).
890 **(H)** Immunofluorescence of PAX7 with LAMININ on sections of TA muscles from male WT and
891 *Dusp13* KO mice, 7 days post-CTX injury. Nuclei are stained with DAPI. Scale bar: 100 µm. The area
892 in the white dotted boxes is shown at a higher magnification. Scale bar: 25 µm.
893 **(I)** Average number of PAX7 (+) nuclei in **(H)** are quantified (n = 3–4 independent experiments).
894 **(J)** Immunofluorescence of MYOGENIN with LAMININ on sections of TA muscle from male WT
895 and 13 KO mice, 7 days post-CTX injury. Nuclei are stained with DAPI. Scale bar: 100 µm. The area
896 in the white dotted boxes is shown at a higher magnification. Scale bar: 25 µm.
897 **(K)** Average number of MYOGENIN (+) nuclei in **(J)** are quantified (n = 3–4 independent
898 experiments).
899 All data are presented as mean ± standard error of the mean (SEM)
900 P values calculated using Student's t-test; n.s., not significant.
901
902

Figure 3 (Hayashi et al.)

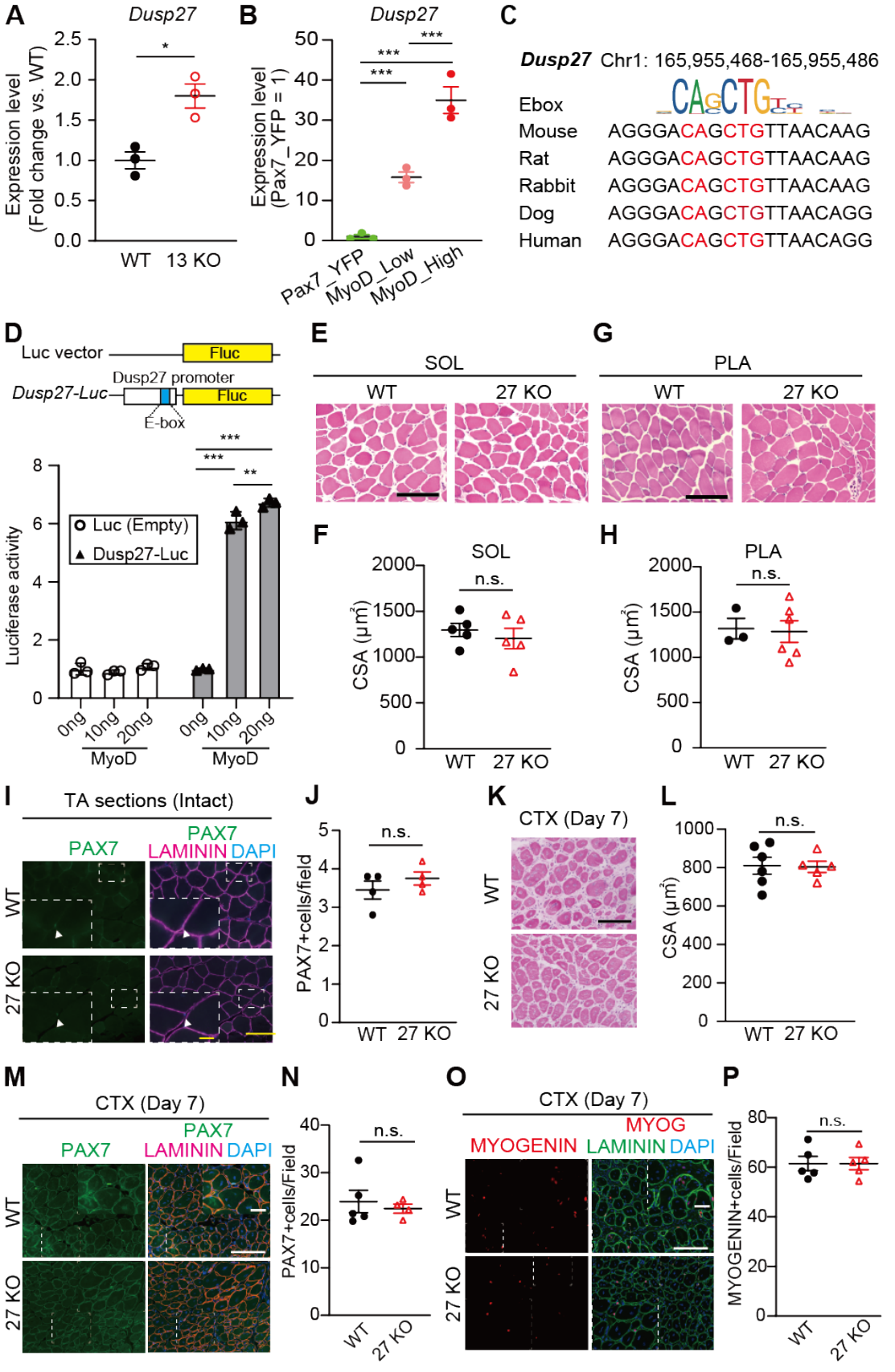

903

904 **Figure 3. *Dusp27* KO mice exhibit comparable muscle development and regeneration to WT**
905 **mice.**
906 **(A)** qPCR analysis of *Dusp27* mRNA levels in gastrocnemius muscles of male WT and 13 KO mice
907 at 12 weeks (n = 3 per group).
908 **(B)** Gene expression of *Dusp27* in RNA-seq data from Pax7-YFP, MYOD-low, and MYOD-high
909 groups (n = 3 per group).
910 **(C)** Ebox-like sequences in the promoter region of *Dusp27* in mammalian species.
911 **(D)** Luciferase reporter constructs of *Dusp27* upstream region (−1,000 to +200) containing an Ebox-
912 like sequence (Top). Relative *Dusp27*-luciferase reporter activities in HEK293T cells overexpressing
913 MyoD (Bottom) (n = 3 per group).
914 **(E, G)** H&E staining of SOL and PLA muscle cross-sections. Scale bar: 100 μm.
915 **(F, H)** CSA of SOL **(F)** or PLA **(H)** muscles of male *Dusp27* KO (27 KO) and WT (n = 3–6
916 independent experiments) mice at 12 weeks.
917 **(I)** Immunofluorescence of PAX7 and LAMININ in intact TA muscles. Scale bar: 100 μm. The area
918 in the white dotted boxes is shown at a higher magnification. Scale bar: 25 μm.
919 **(J)** Average number of PAX7 (+) nuclei in DAPI (+) in **(I)**.
920 **(K)** H&E staining of TA muscle cross-sections of male 27 KO and WT mice at 12 weeks (n = 5–6
921 independent experiments), 7 days post-cardiotoxin injury. Scale bar: 100 μm.
922 **(L)** CSA of damaged TA muscles.
923 **(M, N)** Immunofluorescence of PAX7 **(M)** or MYOGENIN **(N)** with LAMININ on sections of TA
924 muscles from male WT and 27 KO mice, 7 days post-CTX injury. Nuclei are stained with DAPI. Scale
925 bar: 100 μm. The area in the white dotted boxes is shown at a higher magnification. Scale bar: 25 μm.
926 **(O, P)** Average number of PAX7 (+) or MYOGENIN (+) nuclei in **(O)** and **(P)** are quantified (n = 5–
927 8 independent experiments).
928 All data are presented as mean ± standard error of the mean (SEM)
929 P values calculated using Student's t-test, Tukey's test, and edge R; *P < 0.05, **P < 0.01, ***P <
930 0.001, n.s., not significant.
931
932

Figure 4 (Hayashi et al.)

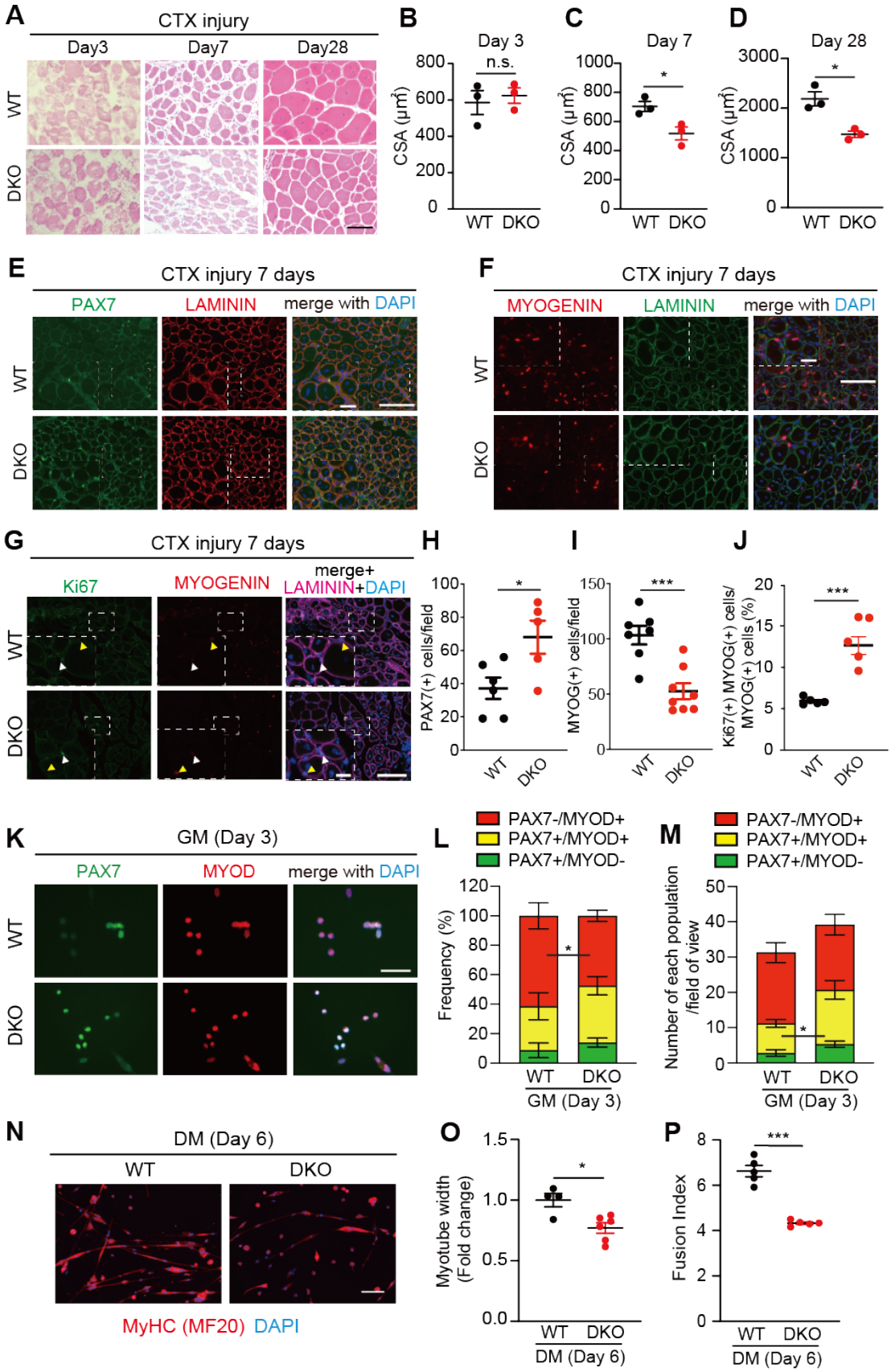

933

934 **Figure 4. Loss of both *Dusp13* and *Dusp27* impairs muscle regeneration after acute muscle**
935 **injury.**
936 **(A)** Hematoxylin and eosin (H&E) staining of tibialis anterior (TA) muscle cross-sections of male
937 *Dusp13* and *Dusp27* double knock-out (DKO) (n = 3) and WT (n = 3) mice at 12–15 weeks of age, 3,
938 7, and 28 days post-cardiotoxin (CTX) injury. Scale bar: 100 μm.
939 **(B–D)** Cross-sectional area (CSA) of damaged TA muscles at indicated time points.
940 **(E, F)** Immunofluorescence of PAX7 (**E**) or MYOGENIN (**F**) with LAMININ on sections of TA
941 muscles from male WT and DKO mice, 7 days post-CTX injury. Nuclei are stained with DAPI. Scale
942 bar: 100 μm. The area in white dotted boxes is shown at a higher magnification. Scale bar: 25 μm.
943 **(G)** Iimmunofluorescence of KI67 and MYOGENIN with LAMININ on sections of TA muscles from
944 male WT and DKO mice, 7 days post-CTX injury. Nuclei are stained with DAPI. Scale bar: 100 μm.
945 The area in white dotted boxes is shown at a higher magnification. Scale bar: 25 μm. White arrowhead
946 indicates KI67+/MYOGENIN+ cells. Yellow arrowhead indicates KI67-/MYOGENIN+ cells.
947 **(H, I)** Average number of PAX7 (+) or MYOGENIN (+) nuclei in **(E)** and **(F)** are quantified (n = 5–
948 8 independent experiments).
949 **(J)** Frequency of Ki67 (+) nuclei in MYOGENIN (+) in **(G)** are quantified (n = 5 per group)
950 **(K)** Immunofluorescence of PAX7 and MYOD on cultured MuSCs from female WT and DKO mice.
951 Nuclei are stained with DAPI. Scale bar: 100 μm.
952 **(L, M)** Quantification of the proportion **(L)** and numbers **(M)** of MuSCs undergoing self-renewal
953 (PAX7 (+), MYOD (-)), activation (PAX7 (+), MYOD (+)), and differentiation [PAX7 (+), MYOD
954 (-)] in (**K**). (n = 6 independent experiments)
955 **(N)** Immunofluorescence with an antibody against myosin heavy chain (MyHC) on MuSCs
956 differentiated for six days in DM. Nuclei are stained with DAPI. Scale bar: 100 μm.
957 **(O, P)** Myotube width **(O)** and Fusion index (numbers of myonuclei per MyHC (+) myotube) **(P)** in
958 **(N)** are quantified (50 myotubes analyzed per experiment).
959 All data are presented as mean ± standard error of the mean (SEM). P values calculated using Student's
960 t-test; *P < 0.05, **P < 0.01, ***P < 0.001, n.s., not significant.
961
962

Figure 5 (Hayashi et al.)

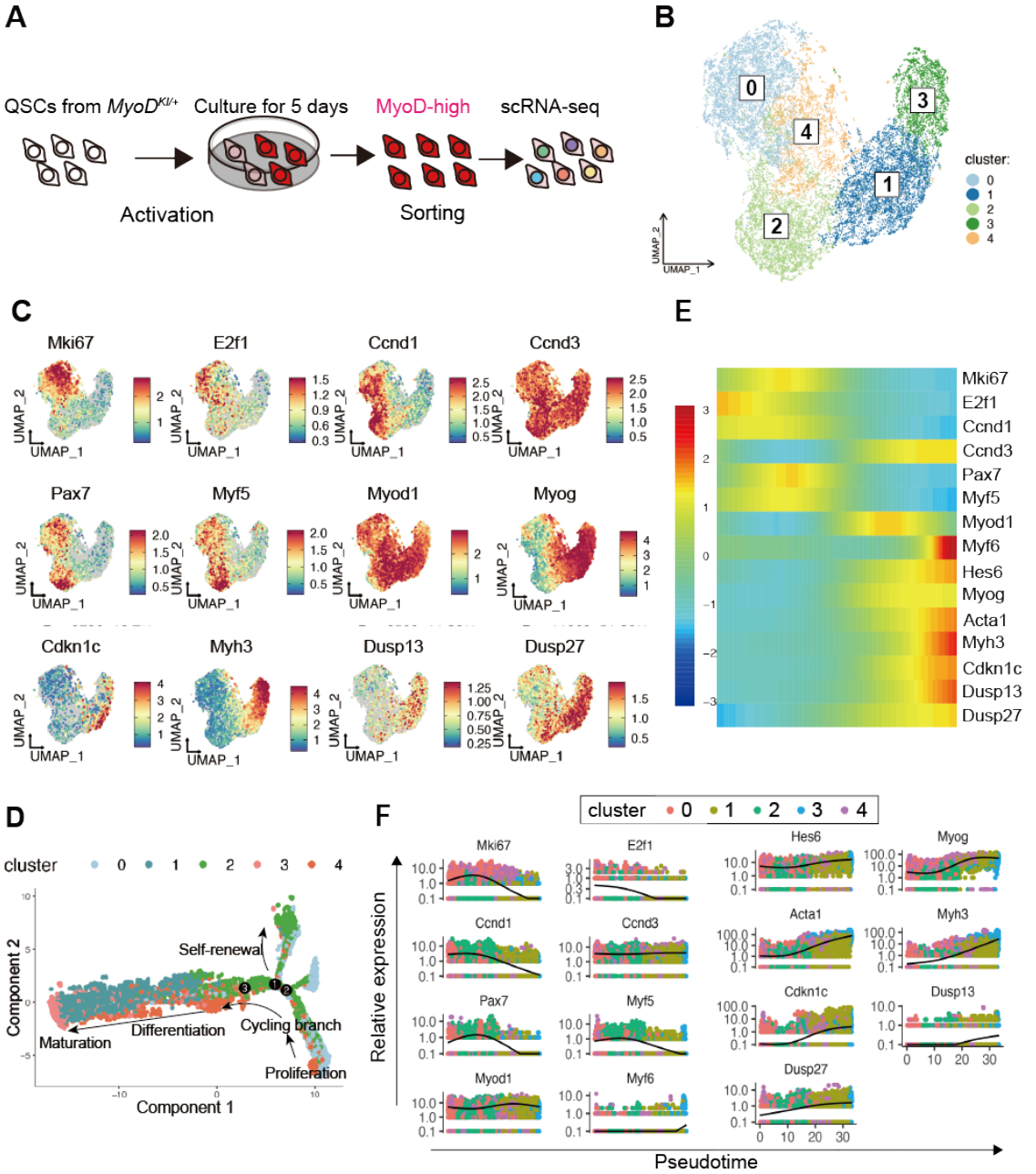

Figure 5. Single-cell RNA-sequencing analysis of MyoD-high MuSCs from MyoD-KI mice reveals *Dusp13* and *Dusp27* expression in the late stage of MuSCs.

(A) Schematic diagram illustrating the scRNA-seq analysis of MyoD-high MuSCs from MyoD-KI mice.

(B) Transcriptomic atlas and clustering of the subset of MyoD-high MuSCs from MyoD-KI mice.

(C) Single-cell expression pattern of the target genes.

(D) Pseudotime analysis performed using the Monocle package. The plot depicts the hierarchy of

MyoD-high MuSCs in the pseudotime trajectory.

(E) A heatmap showing the expression of representative genes in the pseudotime analysis. Each column represents a cell, and each row represents a gene.

(F) Pseudotime-ordered single-cell expression of representative genes.

Figure 6 (Hayashi et al.)

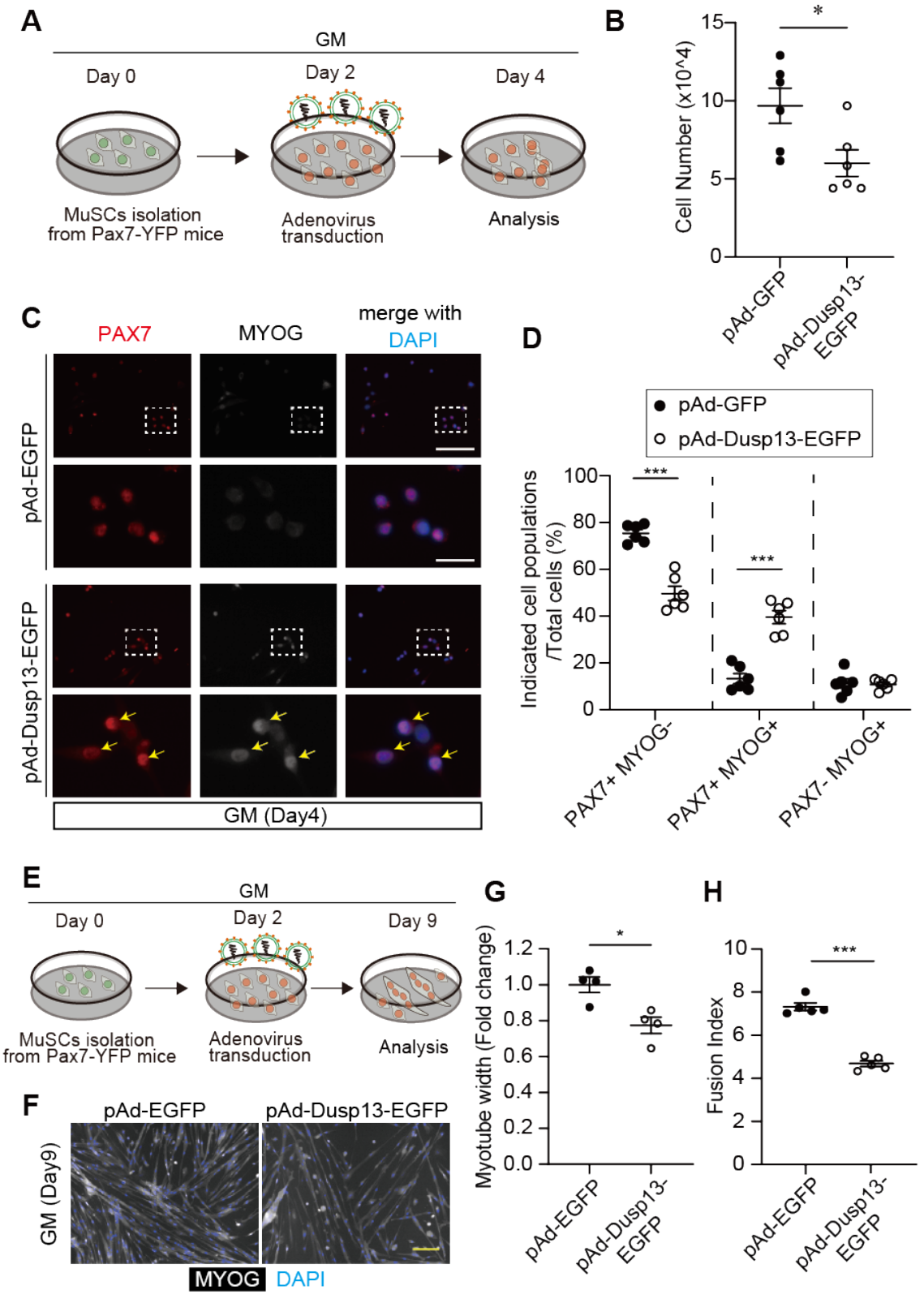

978

979 **Figure 6. Overexpression of *Dusp13* induces precocious muscle differentiation independent of**
980 **phosphatase activity.**
981 **(A)** Schematic diagram illustrating adenovirus infection into MuSCs from 15–16-week-old male
982 Pax7-YFP mice on day 4 of growth medium (GM) culture.
983 **(B)** Number of cultured MuSCs after transduction with adenovirus vectors overexpressing GFP (pAd-
984 EGFP) or Dusp13 (pAd-Dusp13-EGFP).
985 **(C)** Immunofluorescence staining of PAX7 and MYOGENIN in cultured MuSCs after transduction
986 with adenovirus vectors overexpressing GFP (pAd-EGFP) or Dusp13 (pAd-Dusp13-EGFP) on GM
987 day 4. Nuclei are stained with DAPI. The yellow arrow indicates PAX7 (+)/MYOGENIN (+) cells. (n
988 = 6 per group). Scale bar: 100 μm (Upper); 25 μm (Bottom).
989 **(D)** The proportion of each population in (**C**).
990 **(E)** Schematic diagram illustrating adenovirus infection into MuSCs from 15–16-week-old male Pax7-
991 YFP mice on GM day 9.
992 **(F)** Immunofluorescence staining of MYOGENIN in cultured MuSCs after transduction with
993 adenovirus vectors overexpressing GFP (pAd-EGFP) or Dusp13 (pAd-Dusp13-EGFP) on GM day 9.
994 Nuclei are stained with DAPI. Scale bar: 100 μm
995 **(G, H)** Myotube width **(G)** and Fusion index (numbers of myonuclei per myotube) **(H)** in **(F)** are
996 quantified (50 myotubes analyzed per each experiment)
997 All data are presented as mean ± standard error of the mean (SEM). P values calculated using Student's
998 t-test; *P < 0.05, **P < 0.01, ***P < 0.001, n.s., not significant.